Event-related variability is modulated by task and development

Shruti Naik, Parvaneh Adibpour, Jessica Dubois, Ghislaine Dehaene-Lambertz, Demian Battaglia

Contents lists available at ScienceDirect

NeuroImage

journal homepage: www.elsevier.com/locate/neuroimage

Event-related variability is modulated by task and development

Shruti Naik[a], Parvaneh Adibpour[a], Jessica Dubois[a,b], Ghislaine Dehaene-Lambertz[a,*], Demian Battaglia[c,d,*]

[a] Cognitive Neuroimaging Unit U992, NeuroSpin Center, F-91190 Gif/Yvette, France
[b] Université de Paris, NeuroDiderot, Inserm, F-75019 Paris, France
[c] Institute for System Neuroscience U1106, Aix-Marseille Université, F-13005 Marseille, France
[d] University of Strasbourg Institute for Advanced Studies (USIAS), F-67000 Strasbourg, France

article info

Keywords:
Spontaneous activity
Neural variability
Dynamical systems
EEG dynamics
Early infancy
Vision

abstract

In carefully designed experimental paradigms, cognitive scientists interpret the mean event-related potentials (ERP) in terms of cognitive operations. However, the huge signal variability from one trial to the next, questions the representability of such mean events. We explored here whether this variability is an unwanted noise, or an informative part of the neural response. We took advantage of the rapid changes in the visual system during human infancy and analyzed the variability of visual responses to central and lateralized faces in 2-to 6-month-old infants compared to adults using high-density electroencephalography (EEG). We observed that neural trajectories of individual trials always remain very far from ERP components, only moderately bending their direction with a substantial temporal jitter across trials. However, single trial trajectories displayed characteristic patterns of acceleration and deceleration when approaching ERP components, as if they were under the active influence of steering forces causing transient attraction and stabilization. These dynamic events could only partly be accounted for by induced microstate transitions or phase reset phenomena. Importantly, these structured modulations of response variability, both between and within trials, had a rich sequential organization, which in infants, was modulated by the task difficulty and age. Our approaches to characterize Event Related Variability (ERV) expand on classic ERP analyses and provide the first evidence for the functional role of ongoing neural variability in human infants.

Introduction

Since Wundt (1832-1920), the purpose of psychology has been to decompose complex cognitive functions into simpler processes, or mental operations, that could be studied in relative isolation thanks to the careful manipulation of experimental parameters (Posner and DiGirolamo, 2000; Zylberberg et al., 2011). Following this ambition, thousands of studies have been published each year in which the peaks and troughs of average, stimulus-locked neural time-series (i.e. Event-Related Potentials: ERPs) have been explained as neural correlates of cognitive operations. It is indeed quite remarkable that averaging neural signals across multiple presentations of the same stimulus recovers robust and reproducible responses across participants. The ERP literature has progressively identified specific neural components whose latency and scalp-topography have been related to particular cognitive operations, from sensory processes (e.g. recognition of faces: N170; Ghuman et al., 2014), to high-level processes (e.g. detecting lexicon incongruencies: N400; Kutas and Federmeier, 2000), or monitoring our own behavioral errors (ERN: Error Related Negativity; Dehaene et al., 1994).

In this framework, the ongoing/background activity is considered as an unwanted noise discarded through the averaging process (Jasper, 1937). While measurement errors and artefacts are indeed unwanted, the trial-by-trial variation of the recorded signal could also be a genuine property of the participant's brain. Furthermore, since complete cognitive processes take place within each individual trial, and mental operations can vary from one trial to the next (e.g. stimulus visibility at threshold, confidence variation, change of strategy, etc.), the signature of these operations should be detectable within individual trials –without averaging. This methodological tour-de-force is sometimes accomplished by powerful time-series pre-processing or machine learning algorithms (Vahid et al., 2020; Jung et al., 2001). However, all these methods implicitly assume that the pertinent ERP is a weak signal sunk in uncorrelated noise. Is this tenet itself as straightforward as it seems?

An increasing number of studies suggest that the background activity fluctuations are part of the cognitive process itself and can bias perceptual reports and affect stimulus detection (Hesselmann et al., 2008; Sadaghiani et al., 2009). Specifically, the oscillatory components

* Corresponding authors (shared last and corresponding authorship).
E-mail addresses: ghislaine.dehaene-lambertz@cea.fr (G. Dehaene-Lambertz), demian.battaglia@univ-amu.fr (D. Battaglia).

https://doi.org/10.1016/j.neuroimage.2023.120208.
Received 2 March 2023; Received in revised form 11 May 2023; Accepted 30 May 2023
Available online 31 May 2023.

of the background activity, notably in the alpha band (8-12 Hz), have long been known to be suppressed at stimulus presentation (Adrian and Matthews, 1934). Furthermore, pre-stimulus power is inversely correlated with behavioral performance (Van Dijk et al., 2008). Nonetheless, these oscillations are never completely suppressed, and such ongoing oscillations display rich phase dynamics that play an important role in top-down cognitive processes (Palva and Palva, 2007; Klimesch, 2012; Michalareas et al., 2016) and contribute to the emergence of the ERP itself (Hanslmayr et al., 2007). Beyond phase reset, post-stimulus activity and ongoing fluctuations do not simply add up but nonlinearly interact (He, 2013) explaining the resulting perception (VanRullen et al., 2011; Baria et al., 2017). Finally, similarities between spontaneous and stimulus-related activity increase along development (Kenet et al., 2003), possibly suggesting that such spontaneous activity might encode the structure of the environment as priors (Berkes et al., 2011; Pezzulo et al., 2021). In such an alternative framework, brain activity is thought to be sampling a high-dimensional space of possible neural configurations (Mazor and Laurent, 2005; Gu et al., 2018). Such brain activity is considered to unfold along trajectories that are seemingly erratic and stochastic, and yet are loosely shaped by a latent dynamical landscape defined by attractor valleys and ridges connecting them (Chaudhuri et al., 2019). Spontaneous activity can thus organize in reproducible microstates which are visited in complex sequences, differing from mere random walks (Van de Ville et al., 2010). This irregular activity can still be modulated by the task demands, arousal, vigilance, etc. at the moment of stimulus presentation (Huk et al., 2018).

Compatible with this scenario, it was observed that inter-trial variability (which reflects the background activity fluctuations) is not constant but is characteristically reduced in the post-stimulus period with respect to baseline at rest. This *variability quenching* (VQ) after stimulus presentation is a cortex-wide phenomenon robustly observed at many spatiotemporal scales and across many different tasks (Churchland et al., 2010; Arazi et al., 2017; Wainio-ThebergeS and Northoff, 2021). Although different mechanisms may be responsible for it at different scales –e.g. change in excitatory/inhibitory synaptic currents at the micro-scale (Hensch and Fagiolini, 2005; Hennequin et al., 2018) or power increase or phase reset of ongoing oscillations at the macro-scale (Van Diepen et al., 2015; Iemi et al., 2019; Daniel et al., 2019), the net functional effect in all cases is similar and corresponds to an increased reproducibility of neural trajectories, which, in human adults, can be further improved by active attention (Broday-Dvir et al., 2018; Arazi et al., 2019) or conscious awareness (Schurger et al., 2015). Further evidence is nevertheless needed to understand whether this variability reduction is an epiphenomenon or plays a direct role in information processing. We argue that if variability modulations are functionally important (rather than noise), they should have a temporal structure as is the case with ERPs and this structure should emerge relatively early in life. Moreover, this phenomenon might get progressively more complex along development, reflecting the scaffolding of perceptual and cognitive processes.

To test our hypothesis, here we sought to understand the organization of response variability in 5 to 24-week-old human infants as well as in adults when they were presented with human faces. We chose to study this question in human infants for three reasons: Firstly, because during the first semester of life, rapid maturation takes place in the visual domain (Braddick and Atkinson, 2011), allowing age to be used as a factor to separate different neural/cognitive processes that might overlap in more mature brains such as in adults. The second reason is the observation that human infants are exceptional learners (Dehaene-Lambertz and Spelke, 2015). If variability modulation is an intrinsic part of the building and manipulation of internal models, the fast learning pace of infanthood might reveal more complex dynamical changes than the adults who possess relatively stable internal models. Finally, it is a common belief to disregard ongoing activity as a nuisance that compromises the robustness and reproducibility of infant ERPs. We might thus miss important information on the potential structure of the variability modulation in single-trial responses that might lead to better hypotheses and tools to gauge infant cognition.

Using multivariate pattern analysis to track systems level variability induced by visual stimuli, we show that both across and within-trial variability has a complex organization that gradually evolves through early infancy, which by the second trimester of life, reaches a spatiotemporal structure remarkably like that of adults. Moreover, applying our measures of variability for the same infants observing easy and difficult stimuli, we show that stimulus-driven modulations of variability are not only dependent on structural changes of their brain since the same infant is able to flexibly modulate neural variability depending on the task demands. Finally, through distinct but converging analyses of alpha oscillations and microstate transitions, we find that visual stimuli do not induce a sharp reset of system's dynamics but modulate trial trajectories by affecting the speed of topography reconfiguration (independently from the single-trial topographies which can eventually be very diverse).

Taken together, our results suggest that the stimulus does not impact "where the system is" as much as it impacts "how the system flows" after stimulus presentation. We propose the term *Event-Related Variability* (ERV) to collectively describe this remarkable sequential and task-specific organization of variability quenching and boosting events, both between and within trials, which complements the classic descriptions of the modulations of average response (ERP). Such nontrivial ERV dynamics reveals an immediate richness of structured states in infants comparable to adults, confirming a potential role of variability modulations as a computing resource since the earliest ages.

Materials and methods

In this study, we re-analyzed high-density (128 channels) Electroencephalography (EEG) data previously reported by Adibpour et al. (2018) and compared our results with adults performing the same paradigm. Adult data were acquired independently from the infant data and have never been published. We derived three novel measures based on multivariate pattern analysis to track the single trial dynamics and variability induced by the visual stimuli: First, we sought to quantify how individual trial trajectories approach the well-known ERP components (referred hereafter as *ERP flybys*). This allowed us to evaluate how the single-trial distributions of latency and distances to the ERP templates develop during the first semester of life in comparison to adults. Secondly, we examined the *between-trial variability* to quantify how close (or far) individual trial trajectories remained from each other as they evolved through time. This corresponds to the variability quenching phenomenon described earlier. Thirdly, we introduced a novel metric of instantaneous rate of brain state reconfiguration i.e. *Within-trial speed* to track the moment-to-moment fluctuations along individual trials. Finally, as activity fluctuations have oscillatory components, we also studied how the dynamics of the three metrics above relate to alpha (and slower) oscillatory dynamics and, specifically to alpha phase reset, since stimulus-induced alpha phase reset has been proposed as one of the mechanisms for variability quenching (Iemi et al., 2019; Foxe and Snyder, 2011).

Participants

The reported results included data from two cohorts. The first group of healthy full-term infants (N = 39, Mean age: 14. 15 ± 4. 79 weeks, age range: 5. 6 to 23. 6 weeks, 11 girls) was studied elsewhere to investigate the functional maturation of visual Event Related Potentials (ERP) to lateralized faces (Adibpour et al., 2018). A subset of these infants (N = 22, Mean age: 14 ± 4. 96 weeks, age range: 5. 6-22 weeks, 7 girls) was also tested to study ERP responses to central faces. To compare the results obtained for infants with adults, we additionally included a second group of young adults (N = 13, Mean age: 23. 39 ± 2. 32 years, age range: 21 to 27. 1 years, 6 females) who were presented with the

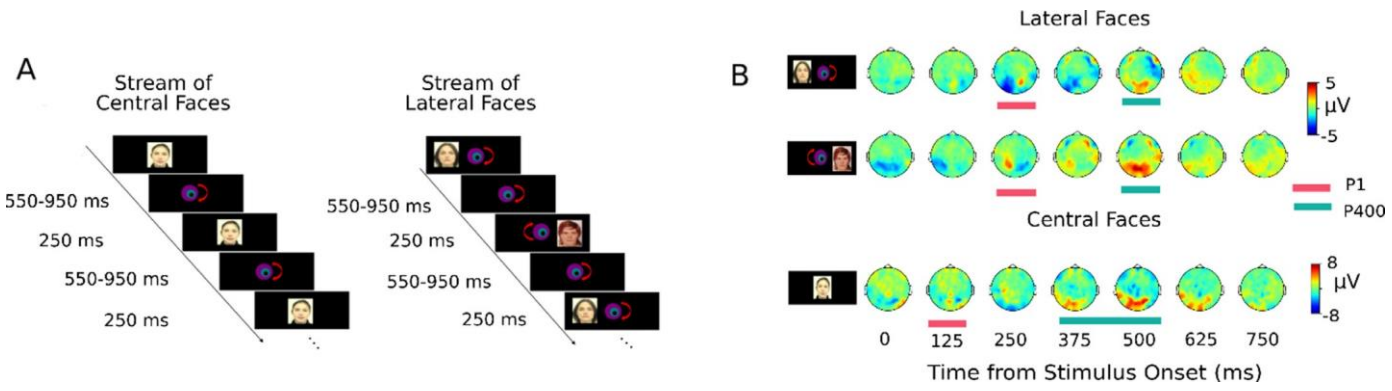

Fig. 1. Task Paradigm and Infant visual ERPs. A) Infants (and adults) were presented with unfamiliar faces consecutively in the left and right hemi-field. A subset of infants was also presented with faces in center. **B)** Grand Average voltage topographies for the three conditions for infants (without baseline correction). Early (P1) and late (P400) ERP components (marked with red and green horizontal bars respectively) are visible for each condition.

lateralized faces following the same paradigm as infants. To further investigate the maturation effect in some of the analyses, we split the data, and contrasted the youngest (<12weeks, N = 14) with the oldest infants (>16 weeks, N = 13), because the first trimester (<12 weeks) is a period of rapid maturation of the visual pathways, from the retina to V1 in term of cell maturation, tracts myelination and synaptogenesis leading to drastic changes in visual perception followed by slower changes (Dehaene-Lambertz and Spelke, 2015). This study has been approved by the Comité de Protection des Personnes (CPP) Ile de France VII and was authorized by the AFSSAPS under the reference ID-RCB 2011-A00058-33. All adult subjects and parents of infants gave written informed consents before participating in the study.

Experimental paradigm

For the lateralized faces, the experiment started by a rotating colored bull's-eye that remained at the center of the screen during the whole experiment to attract infants' attention to the center of the screen. Streams of face images (male or female face out of 6 neutral, unfamiliar front faces) appeared consecutively on the left and right side of the bull's eye for 250ms followed by a random delay between images (550 to 950ms post-offset of the image with a 50-ms step). The random delay ensured minimal anticipatory gaze to the left or right side. For central faces, one female and one male face, not used during the lateralized paradigm, were presented at the center of the screen for 250ms, spaced by a random interval of 550-950ms during which the colored bull's eye was presented. Fig. 1A summarizes the task paradigm.

EEG protocol and pre-processing

EEG recordings were acquired with EGI net comprising 128 electrodes for infants and 256 electrodes for adults and digitized in real-time at a sampling rate of 250 Hz. EEG data were further pre-processed in EEGLAB software. Recordings were band-pass filtered between 0. 5 and 20 Hz. The choice of low-pass cutoff was guided by the previous observation that upto 54 weeks of age, only ~2-4% of total band-limited power was concentrated in frequencies >10Hz (Marshall et al., 2002). The signal was further segmented into epochs of 1. 9 s (−0. 4 to 1. 5s relative to the onset of face presentation). Channels and trials contaminated by motion or eye-blink artifacts were automatically rejected (after epoching) by an algorithm developed to detect abrupt changes as large drifts within each trial (>150 μv). Electrodes were rejected for the entire recording if they were detected as "bad" in more than 70% of the epochs. Trials were rejected if half of the electrodes were marked bad (see Table S1 for numbers of retained and rejected trials). For infants, additional trials were rejected when the eye-gaze moved away from the central attractor by inspection of video-recordings. Epochs were re-referenced by reference averaging, but no baseline correction was applied to allow unbiased analyses of post-stimulus variability as compared to pre-stimulus variability. Finally, EEG topographies were normalized by dividing the activity of each sensor by the global field power (GFP, i.e. standard deviation across sensors) at each time-point. This step was performed to avoid confounding variability analyses by the absolute voltage magnitudes (signal strength / SNR) on each sensor as recommended in the literature for topographic pattern matching analyses (Skrandies, 1990).

For the three event-related variability (ERV) matrices (i.e. Flyby, between-trial variability and within-trial speed), temporal smoothing was applied by averaging the activity at each sensor in a 100-ms overlapping sliding window centered at a given time point in each trial, to capture single trial effects that are robust against sudden jumps in topographies due to faulty sensors or external noise. However, all the three variability analyses were repeated without this temporal smoothing as well as for one shorter (20ms) and one larger window size (180ms), yielding very similar results (Fig. S7). By design, there were fewer trials for central faces as compared to lateral faces (cf. Table S1). Hence, we made sure that comparisons between these conditions were not confounded by the difference in trial numbers by downsampling the trials of lateral faces condition to match with the central faces condition when pertinent. Additional information about data acquisition, pre-processing and task paradigm not pertaining to the current study is detailed in Adibpour et al. (2018).

Microstates analysis and trajectory in principal components (PC) space

To derive combined microstates for infants, we used K-means clustering on concatenated multivariate EEG signals, ignoring bad segments. The number $n = 4$ of microstates was selected for comparison with previously reported results (Michel and Koenig, 2018). Using the microstate templates as cluster centroids, we determined the closest microstate template for all instantaneous topographies, that is, the one with the least correlation distance (1- Pearson correlation). Symbolic sequences of microstate transitions (labeled from "A" to "D") were further segmented into epochs to align them to stimulus onset times. Every microstate transition (irrespectively of the specific microstates involved) was labeled as a "spike" (a point process event occurring at a specific time t) and generic microstate transition rates were estimated convolving trains of transition events with a 100ms smoothing Gaussian kernel. These smooth transition curves were averaged across trials to convert the transition trains into transition probabilities. We also estimated probabilities of observing specific microstates, evaluating the fraction of trials the system was in each given microstate in a given peristimulus-time bin across stimulus-aligned trials, pooling over all subjects.

For one example subject, we projected a 12s long segment of clean, continuous, smoothed (100 ms sliding window) EEG data containing 10 consecutive (left and right faces) trials using a standard principal component (PC) analysis. The 128-dimensional signal segment was thus projected for visualization on the three-dimensional space spanned by the first three PCs (explaining 82% of signal variance).

Extracting ERP templates

For each condition (left, right and central) and for each cohort (infants and adults), we derived grand average ERP topography by averaging subject-specific ERP activity separately for each sensor across subjects (Fig. 1B for infants, Fig. S1A for adults). For infants, we identified 'P1 template' as grand-average topography in the range of ~225-275ms post-stimulus for lateralized faces and in the range of ~125-175ms post-stimulus for central faces. Similarly, 'P400-template' was derived as the average topography in the range of ~525-575ms post-stimulus for both lateral and central faces (Fig. S3 A). For adults, we identified 'P1 template' as the grand average topography in ~75-125ms post-stimulus while 'P400 template' was identified as ~375-425ms post-stimulus (Fig. S3 B). These time-ranges were chosen by selecting a 50ms long time-window around the peak of the global field power (GFP) in grand-averaged ERP topography as inspected visually (Fig. 1B).

Measures of trial-variability (i.e. flyby to known ERP templates, between-trial variability and within-trial speed) were calculated as topographic dissimilarity using spatial correlation distance (1- Pearson correlation coefficient) as dispersion metric. Hence, absolute distances varied from 0 (absolute positive correlation) to 2 (negative correlation). Correlation distance decouples the topographic patterns from their magnitudes, allowing focusing on the relative spatial patterns rather than their absolute magnitudes.

'Flyby' to ERP templates

For each subject and for each condition, flyby distance from trial t to a certain ERP template Φ at time t was calculated as correlation distance,

$$\Delta(t, \Phi) = 1 - CC(X, \Phi(t, \Phi))$$

Where, $CC(t, \Phi)$ denotes Pearson's correlation coefficient and $\Phi(t, \Phi)$ represents topography at trial t and time t. These single-trial distance time-series were further averaged across trials for each ERP template to obtain a single time-series per subject for P1 and P400 templates and for each condition (Fig. 3 A).

'Fly-by' Latency and Distance: In the predefined time range for each ERP template, moments of closest 'flybys' to these templates were identified as the time-points when the distance $\Delta(t, \Phi)$ fell into the lowest 5 percentile of the overall distance distribution. Latency of these moments was used for the analyses of median and jitter in flyby latencies for each infant (Fig. 3B, Fig. S4C, D). The time-range to derive flybys was restricted to 150-350ms for P1 template and 400-600ms for P400 template in case of lateral faces. For central faces, 0-150ms for P1 template and 350-550ms for P400 template. For adults, the analysis was restricted to 0-150ms for P1 and 150-500ms for P400 template. These time-ranges were chosen based on the lowest flyby distance in the grand-average time-curves. Mean and S. D. of all single-trial flyby distances in these time-ranges were calculated for the comparison across subjects. (Fig. 3C, Fig. S4 E-F).

Since the choice of ERP templates can confound the flyby analyses, various control checks were performed to make sure that these templates represent a reasonable statistical estimate of the true evoked responses. First, all flyby metrics (defined below) for lateralized faces were also reanalyzed with "Subject-specific ERP templates". Whereby, for each subject, the ERP template was defined independently from other subjects (as the average topography at the time of peak of P1 or P400 ERP responses as identified previously in Adibpour et al. (2018). The resulting subject-specific templates were also compared to the grand average ERP-templates to ensure that no specific infants' ERP dominated the grand average ERPs (Fig. S5A). Finally, all flyby analyses were also re-performed by comparing single-trial topographies of subject *i*, to grand-average ERP topography built by excluding the i^{th} subject to account for equal variance from each subject specific ERPs (Fig S5 B, C).

Between-trial variability

For each subject and for each condition, between-trial variability at time t was calculated as the average of all pair-wise spatial correlation distances between all trial-pairs *i* and *j*;

$$\Delta(t) = \frac{1}{\binom{n}{2}} \sum_{i,j} (1 - CC(\Phi(t, i), \Phi(t, j)))$$

Where, n = number of trials, $\binom{n}{2}$ suggests all pair-wise combinations of trials, CC is Pearson correlation coefficient and $\Phi(t, i)$ represents sensor topography at trial i and time-point t.

Absolute single-subject between-trial variability time-courses were derived per condition and further z-scored across time, to obtain relative between-trial variability. These z-scored time-series were further averaged in the previously defined time-range for P1 and P400-flybys to obtain relative between-trial variability around flybys (Fig. 4, Fig. S6).

Topography of Between-trial Variability Quenching: If sensor s has $d(s)$ neighboring channels, between-trial variability is calculated for this sensor at time t as follows:

$$\Delta(s, t) = \frac{1}{\binom{n}{2}} \sum_{i,j} (1 - CC(\Phi_s(t, i), \Phi_s(t, j))$$

Where, CC is Pearson correlation coefficient; $(\Phi_s(t, i))$ is the $d(s) + 1$ dimensional activity vector at time t and trial i, where each dimension represents the activity of a different neighbor of sensor s (including itself). Neighbors of each channel were extracted from the channel-connectivity matrix estimated using the "find_ch_connectivity" function of MNE-python (Gramfort et al., 2013). For each subject, instead of single global between-trial variability time-series, now we obtained one time-series each for each sensor. This absolute sensor-level between-trial variability was further z-scored across time to obtain relative variability for each sensor. These (channel *times* time) matrices for each subject were further averaged to obtain group-level between-trial variability topography (Fig. S8C).

Within-trial speed

For each trial$t$, within-trial speed at time *t* was calculated as spatial correlation distance between topography at that time-point and the same at the consecutive time-point.

$$\Delta(t, i) = 1 - CC(\Phi(t, i), \Phi(t, i + 1))$$

where, CC is Pearson correlation coefficient and $\Phi(t, i)$ represents sensor topography at trial i and time-point$t$. Overall absolute within-trial speed for each subject was obtained by first averaging speed time-courses across trials and then averaging the mean speed time-courses across time (Fig. 5, S10).

Fly-by Triggered Speed Profiles: For each subject, moments of 'fly-by' to known ERP templates were identified as described above (i.e., trial- to-template distance falling in the lowest 5^{th} percentile). Trial-speed segments at each occurrence of 'fly-by' were extracted as speed time-course from 400-ms before to 400-ms after 'fly-by'. Each of these 800-ms long speed time-courses were averaged to obtain a single speed profile per template (Fig. 5B). These subject-specific absolute speed profiles

were z-scored along the time dimension to obtain relative speed profiles around fly-by and further averaged to obtain group-average speed-profiles (Fig. 5B, S10C). To compare flyby triggered instantaneous speed across infants, peak speed (for P1 template) and lowest speed (for P400 template) were identified in the 100ms time-window centered at 'flyby' moment (Fig. S10D-F).

Trial Speed Distribution: To obtain trial-speed distribution for each age-group per condition, all single-trial speed time-courses were concatenated along time and along subjects in that age-group to obtain one single speed distribution. Probability density was obtained by normalizing area under each bin to 1. Normalized bin-counts (density) were plotted on a log-log scale (Fig. S10B).

Quantifying features of ongoing oscillations

To compare ERV measures to oscillatory events, we measured low-frequency oscillatory power and single-trial instantaneous phases of "alpha" (9-12 Hz) oscillations, and then computed phase-synchrony across trials for each subjects using circular variance (CV). Many studies have previously shown that infants and children have considerably slower alpha oscillations than adults (Marshall et al., 2002; Chiang et al., 2011; Hill et al., 2022; Freschl et al., 2022; Stroganova et al., 1999). Therefore, we also repeated all the analyses in a lower frequency band of 4-9Hz (later denoted as "theta" or "infant alpha"). After bandpass filter- ing into the narrow "alpha" or "theta" bands, we applied Hilbert trans- form to the signals to extract envelope amplitude and phase for each channel. Based on the phase time-series, we quantified at every time the standard metric of Circular Variance (CV), as a normalized index of variability in instantaneous phases across stimulus-aligned trials, which varies between 0 to 1, with 1 indicating complete synchrony. We used the envelope time-series as a quantification of narrow-band-specific signal amplitude at each time-point.

Statistics

Linear trends were tested using Pearson's r correlation and the associated p-values were estimated by permutation testing, i.e. largest (lowest) percentile of the null distribution being smaller (larger) than the sample-based r coefficient (1000 replicas). The associated confidence intervals are computed under normality assumption ($\hat{r} \pm z_{0.975} S$, where $\hat{r}$ is the Fisher-transformed correlation coefficient r). Linear regression lines are surrounded by a shaded band, estimated via bootstrap with replacement, such that the "true" regression line is contained within this band with 95% of probability. We also computed rank-based Spearman correlations coefficients, comparing them with corresponding Pearson's r, to confirm their robustness. Note that the small sample size can lead to broad confidence intervals approaching zero indicating weak correlations. Significant reductions in variability time-courses were tested using one-sample t-test and correction for multiple comparisons and temporal non-independence was applied using cluster-based permutation test as implemented in MNE-python (Gramfort et al., 2013). Group-level differences between paired groups of variables (lateral vs central faces) were tested using nonparametric two-tailed Wilcoxon signed rank test. Group differences between age groups were tested using non-parametric Kruskal-Wallis test, followed by pair-wise comparisons using Mann-Whitney U test with Bonferroni correction.

Data availability

The working examples and computational codes for calculating variability measures are publicly available at https://github.com/transpersonify/variability_quenching. Due to ethical reasons, infants and adults EEG data are not yet publicly available. However, pre-processed and original anonymized data can be made available upon reasonable request to Ghislaine Dehaene-Lambertz (ghislaine.dehaene-lambertz@cea. fr).

Results

Event-related potentials (ERP) to faces in infants and adults

Both infants (N = 39, 5-24 weeks) and young adults (N = 13, 21-27 years) were presented with unfamiliar faces, alternatively between the lateral hemi-fields, and for a subset of infants (N = 22, 5-22 weeks), separately in the central visual field (Fig. 1A, cf. Adibpour et al., 2018). Classical ERP analyses revealed two prominent ERP components: an early *"P1"* and a late *"P400"*. These components, commonly identified in infants in response to visual images and particularly faces, correspond to different cognitive stages: P1 is considered as the first cortical response in primary visual areas whereas the P400 is a higher order response related to face perception and stimulus familiarity, with sources in the fusiform region (De Haan et al., 2003; Ghuman et al., 2014). These components, visible in the grand average topography in Fig. 1B for infants, also had clear equivalent topographies in adults (Fig. S1A). For adults, latencies were faster, voltage topographies qualitatively similar and overall ERP signal amplitude weaker as compared to infants. For lateral faces, the P1 response corresponded to the first positivity on the contra-lateral posterior electrodes around 250-300ms following face onset in infants (~100ms in adults). The P400 response was a large bilateral positivity on occipitotemporal clusters following the P1 response around 500-600ms (~400ms in adults).

For central faces, latencies were faster relative to lateralized faces: around 150ms for the P1 visible on medial posterior electrodes and around 450-550ms for the P400 on occipitotemporal channels (Fig. 1B bottom row). The overall signal amplitude was larger for central than for the lateral faces. These results agree with previous literature on ERP dynamics following face presentation in adults and infants. Concerning other ERP components described in the literature, infant "N290" topography was not prominent and adult "N170" topography did not find clear equivalence in infants, hence we avoided these intermediate components.

Ongoing variability dominates ERP

While characteristic ERPs existed, single-trial responses were noisy and hardly resembled grand averaged responses (Fig. 2A; Fig. S1B), typically remaining one- or two- order of magnitude larger than ERP amplitudes in both adults and infants, with extremely variable topographies and no clear peaks or valleys corresponding to the ERP.

To illustrate the relationship between the ongoing and evoked activity, we show a 12 s-long-segment of continuous EEG data for a representative infant (age = 15. 4 weeks) in Fig. 2B. At every time point, brain topography is represented as a point in a three-dimensional projection after dimensionality reduction (performed by applying Principal Component Analysis (PCA) to activity amplitudes, see *methods*). If stimulus presentation always evoked a similar single-trial trajectory, the EEG trajectory time points recorded immediately following the presentation of a face stimulus should cluster together within this low-dimensional projection. On the contrary, post-stimulus trajectory snippets (highlighted in red in Fig. 2B) were distributed nearly uniformly throughout the sampled space. This dispersion suggests that post-stimulus temporal fluctuations of neural trajectory were predominantly determined by the ongoing activity. Individual stimulus presentation events did not lead to a radical reset of the activation topographies and did not flatten them to reproduce grand-average topographies.

Ongoing spontaneous activity has been shown to have a rich spatiotemporal organization, which has been previously characterized in terms of discrete 'Microstate transitions', i.e. switching between transiently stable patterns of scalp topographies (Van de Ville et al., 2010). Here we extracted microstate sequences from EEG recordings as a possible, simple way to apprehend the organization of global ongoing fluctuations. We describe them as transitions between a set of unsupervised reference topographies, which can be thought as an average orienta-

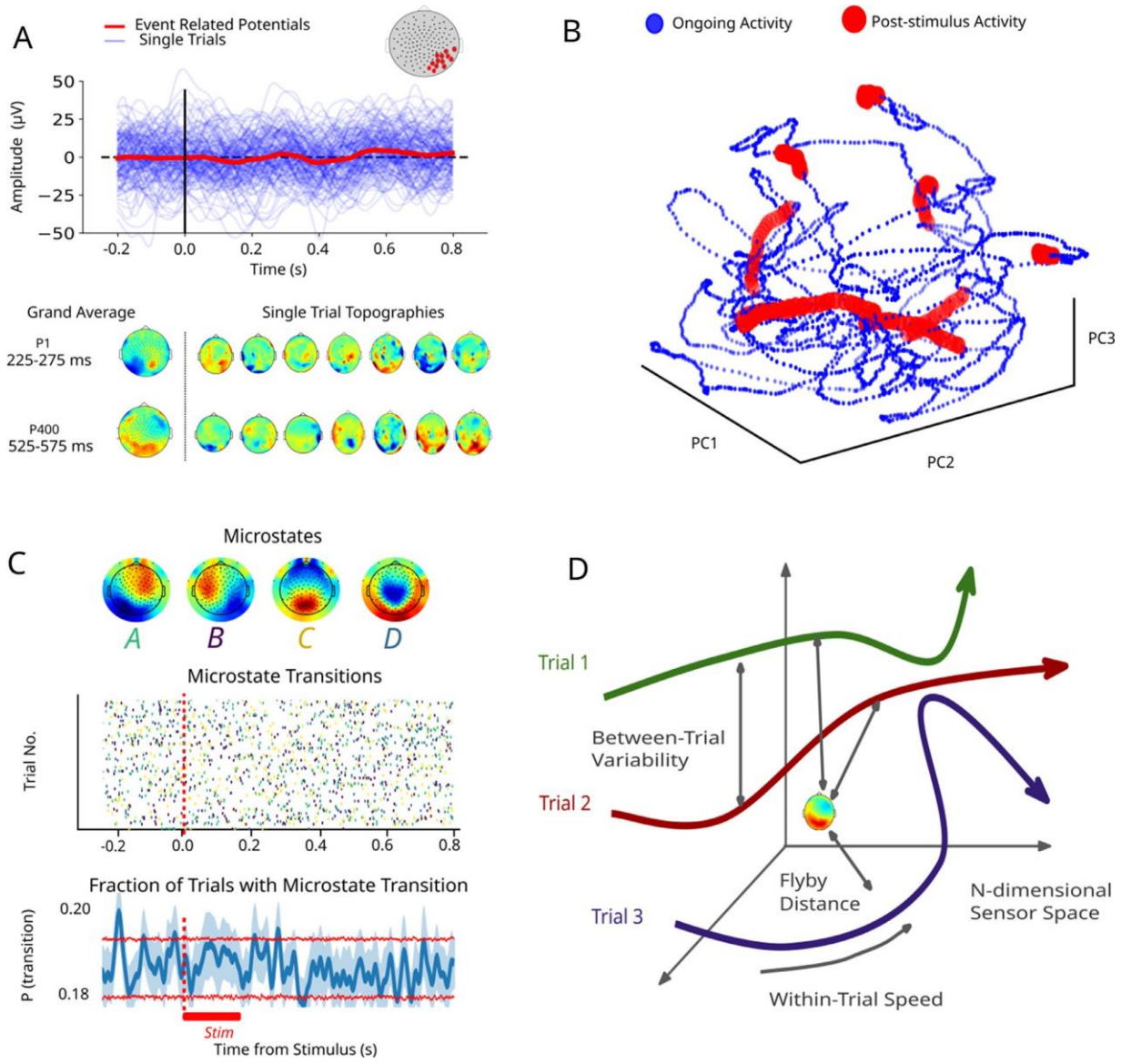

Fig. 2. Ongoing Variability dominates Event Related Potentials. A) Example voltage time-courses averaged across right occipital electrodes for a representative infant (age = 15. 4 weeks) for faces presented in left hemi-field. Amplitude and latency of single-trial responses (blue lines) are highly variable in comparison with average ERP response (red bold line). Single-trial voltage topographies in P1 and P400 response range are notably different from the grand average ERP topography. **B)** Trajectory of continuous time-segment (~ 12 s) reduced to 3-dimensional PC space from 128-channel EEG sensor space for the same infant. Each point corresponds to single instantaneous voltage topography. Time-points falling in the 450-500ms post-stimulus time range are marked in red. **C)** Top sub-panel: Topographies of infant microstates. Middle sub-panel: Raster plots of single-trial microstate transition trains. Each dot marks a change in microstate at that time point. The color of dots indicates which microstate was transitioned into at that time point (corresponding to the colors of letters indicated below the microstate topographies). 100 randomly chosen trials for a representative infant are plotted for visibility. No clear pattern of transitions is visible. Bottoms sub-panel: Gaussian smoothed microstate transition rates averaged across all trials and infants (see Methods). Red horizontal lines represent the 5-th and the 95-th percentile of the distribution of chance-level transition probability (computed through shuffling microstate labels, $N_{permutations}$ = 10000). The absence of peak in this curve shows the microstate dynamics remain unperturbed. **D)** Schematic summary of methods used to gauge single-trial variability: Flyby to ERP templates (how far a trial transits from reference ERP-like configurations); Between-trial variability (how far are single trial trajectories between them); and Within-trial speed (how fast EEG topographies evolve along each trial).

tion frame. We checked whether presentation of the stimulus led to a perturbation of ongoing dynamics, in terms of enhanced probabilities to observe certain microstates or stimulus-triggered microstate transitions (see *Methods*). Fig. 2C (top) shows the four microstates extracted by the standard k-means clustering of the continuous EEG time segments across all infants during the lateralized face paradigm. The topographies were reminiscent of the ones commonly observed for adults in microstate studies. In Fig. 2C (middle panel), we visualize the transitions from one microstate to another as a raster plot, to understand whether the transition probabilities were modified by the stimulus presentation. If microstate transitions became more frequent at a certain fixed post-stimulus latency, one would observe the formation of vertical stripes in this raster (depicting time-aligned transition for each trial) possibly of relatively uniform color (indicating a specific microstate being associated to post-stimulus activity). On the contrary, the raster plot appears unstructured and "asynchronous", with a salt-and-pepper arrangement of colored dots, denoting that stimulus presentation does not induce a strong selection of a specific microstate. As shown in Fig. 2C (bottom panel), the probability of observing a microstate switching transition as a function of peri-stimulus time, all microstate transitions confounded,

Table 1
Average closest flyby distances across age-groups: 5-12 week-old infants (N = 14, first trimester infants); 16-24 week-old infants (N = 13, second trimester infants); and adults (N = 13) were compared using separate Kruskal-Wallis tests for different ERP templates (P1, P400 responses) and for faces presented in the left and right hemi-field. The main effects are reported before post-hoc Mann-Whitney U-test for pair-wise comparisons. P values are corrected for multiple comparisons using Bonferroni correction.

Comparison of P1 and P400 Flyby Mean Amplitude Across Age-Groups		
	Left Faces	Right Faces
P1	H (2) = 11. 48, p = 0. 003 5-12 wo vs 16-24 wo: p = 0. 21n. s. 5-12 wo vs adults: p = 0. 009 16-24 wo vs adults: p = 0. 015	H (2) = 9. 76, p = 0. 007 5-12 wo vs 16-24 wo: p = 0. 34n. s. 5-12 wo vs adults: p = 0. 014 16-24 wo vs adults: 0. 072 n. s.
P400	H (2) = 13. 29, p = 0. 0013 5-12 wo vs16-24 wo: p = 0. 18 n. s. 5-12 wo vs adults: p = 0. 001 16-24 wo vs adults: p = 0. 25 n. s.	H (2) = 13. 47, p = 0. 001 5-12 wo vs 16-24 wo: p = 0. 4 n. s. 5-12 wo vs adults: p = 0. 003 16-24 wo vs adults: p = 0. 028

was not significantly modulated by stimulus presentation. Only when looking at the probabilities of observing specific microstates, we could find some mild modulations (see Fig. S2 for details), nevertheless far from denoting a deterministic reset.

These analyses suggest that the ongoing dynamics is not radically reconFig.d or perturbed by stimulus presentation in its global aspects. On the contrary, stimulus-induced effects appear to be riding on top of ongoing fluctuations. System's trajectories can be virtually "everywhere" in the high-dimensional space of possible topographies and stimulus-related effects must correspond to small local amplitude or phase modulations of current trajectories rather than a radical channeling of the trajectories along specific paths.

With the hypothesis that this tremendous response variability and moment-to-moment fluctuations is informative about underlying neural and cognitive processes, we considered three indicators to detect weak stimulus-related modulations on top of highly variable signals (see cartoon representations in Fig. 2D) as previously described (see *Methods*): *ERP component flybys, between trial variability* and *within-trial variability (or trial Speed).*

Single-trial flybys to classic ERP components are modulated by age

Despite erratic trajectories, grand average ERP topographies are reproducible across studies suggesting they capture stimulus-relevant information. Hence, we analyzed how individual trials approach (or flyby) these "landmark" events. We defined the grand averaged P1 and P400 topographies (separately for infants and adults) as *ERP-templates* (Fig. S3, see *Methods*). The distances to these templates at flyby and the latencies at which the flybys occurred stochastically fluctuated across trials. Therefore, beyond computing average values, we also computed standard deviations of distance and latency across trials. We then assessed whether flyby-related quantities and their variability depended on age (eventually, displaying or not a trend) or stimulus type (lateral vs central faces). A few selected trends are shown in Fig. 3, and additional trends in Fig. S4. Table 1 reports average closest P1 and P400 fly-by distances across age groups. Table 2 reports significant correlations with age of distances and latencies of flybys (we list both Pearson and Spearman correlation values to confirm robustness of results). We comment here briefly, however, on the most remarkable findings.

Firstly, for all task-conditions, individual trial trajectories slightly and significantly reduced their distance to the ERP-templates around specific latencies (distance drops in Fig. 3A and S4A respectively for right and left faces, emphasized by red vertical lines). However, even at these events of closest flyby they remained quite far from the ERP-

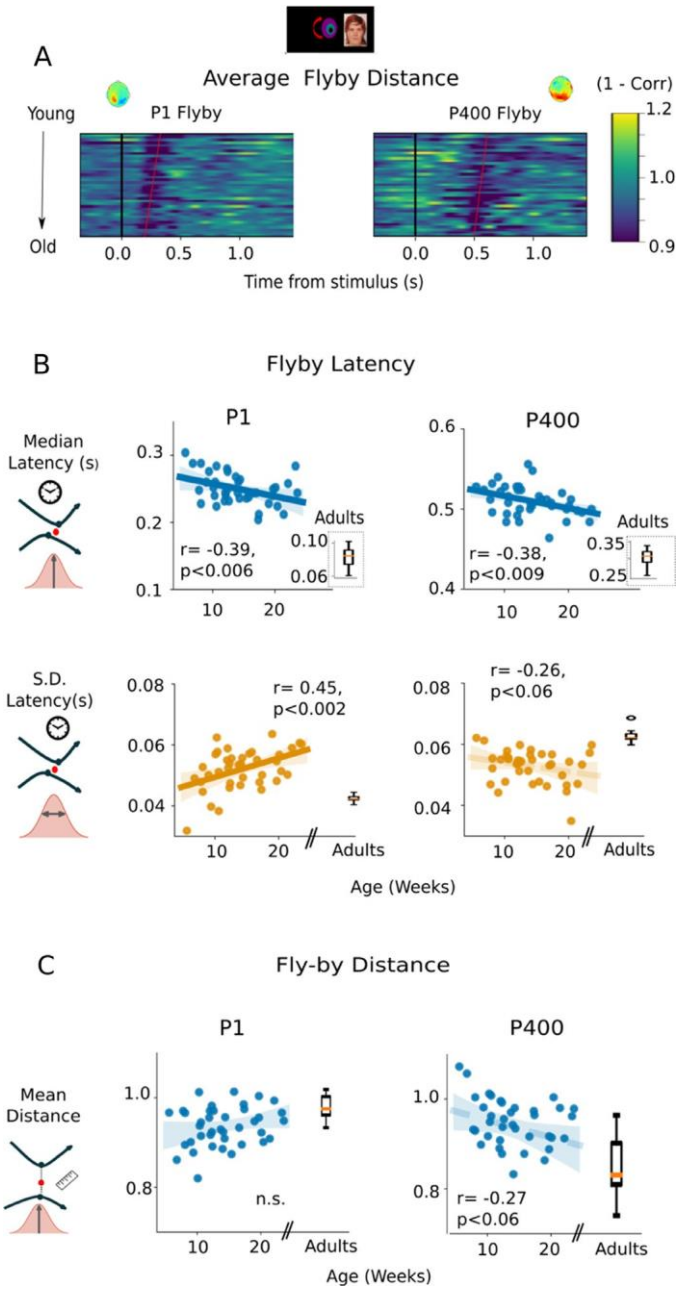

Fig. 3. Maturation of single-trial Flyby statistics for faces presented on the right hemi-field. A) Average flyby distances to P1 (left) and P400 (right) ERP templates (shown on top) for each infant. Each row represents a single infant, sorted in ascending order according to their age (from youngest = 5. 6 weeks to oldest = 23. 1 weeks). Red vertical lines emphasize the reduction in average flyby distance from ~150-350ms for P1 and ~400-600ms for P400 templates. The slopes of red lines suggest that latency of closest distance reduces with age. **B**) Median flyby latency was significantly negatively correlated with age for both P1 (top left) and P400-flyby (top right panel). At the same time, S. D. of single-trial flyby latencies significantly positively correlated with age for P1 (bottom left panel) and showed a negative trend with age for P400 template (bottom right panel). Inset box-plots represent the same statistics for adults. **C**) Average flyby distances to P1 template showed non-significant increase with age (top left panel), while the same for P400 template decreased with age (top right panel). Box-plots indicate that once again adults followed the same trends. Shaded areas indicate 95% confidence interval for regression estimates, all r-values corrected for multiple comparisons with 1-tailed permutation t-test). See Table 2 for correlation values (Pearson and Spearman coefficients) and Fig. S4 for additional scatter plots.

Table 2
Correlation trends with age of latency and distance mean and variability of flybys to P1 and P400 ERP components, for right, left and centrally presented faces. The letter *r* denotes Pearson correlation and the letter □ Spearman rank-based correlation. Only significant correlations are indicated (i.e. 95% confidence interval not containing 0, for both types of correlations). None of the age-correlations of flyby distance mean and variability for the P1 component and of latency variability for the P400 component were significant (hence the missing table rows).

Correlations between ERP fly-by properties and age				
		Right faces	Left faces	Central faces
P1	Latency (mean)	r = -0. 39, p = 0. 006, 95% c. i. [-0. 63, -0. 09]	–	–
		□ = *-0. 36*, *p = 0. 02*, 95% c. i. [-0. 61, -0. 05]	–	–
	Latency (variability)	r = 0. 45, p = 0. 002, 95% c. i. [0. 16, 0. 67])	–	–
		□ = *0. 37*, *p = 0. 003*, 95% c. i. [0. 06, 0. 61]	–	–
P400	Latency (mean)	r = -0. 38, p = 0. 009, 95% c. i. [-0. 62, -0. 07]	–	r = 0. 46, p = 0. 02, 95% c. i. [0. 05, 0. 74])
		□ = *-0. 40*, *p = 0. 007*, *95% c. i. [-0. 63, -0. 1]*	–	□ = 0. 44 (p=0. 01), 95% c. i. [0. 02, 0. 73])
	Distance (mean)	–	r = -0. 35, p = 0. 018, 95% c. i. [-0. 6, -0. 04]	r = -0. 52, p = 0. 006, 95%c. i. [-0. 77, -0. 13]
		–	□ = -0. 33, p = 0. 018, 95% c. i. [-0. 58, -0. 02]	□ = -0. 52, p = 0. 005, 95%c. i. [-0. 77, -0. 13]
	Distance (variability)	r = 0. 34, p = 0. 02, 95% c. i. [0. 03, 0. 59]	r = 0. 42, p = 0. 003, 95% c. i. [0. 12, 0. 65]	r = 0. 53, p = 0. 007, 95% c. i. [0. 14, 0. 78]
		□ = 0. 33, p = 0. 02, 95% c. i. [0. 02, 0. 58]	□ = 0. 39, p = 0. 006, 95% c. i. [0. 08, 0. 63]	□ = 0. 60, p = 0. 003, 95% c. i. [0. 24, 0. 81]

templates, with closest flyby distances close to ~0. 8, i.e. not so far away from the unit value which would correspond to complete lack of correlation (cf. Fig. 3A, Fig. S4A, B). This is in line with the intuition that stimulus induces small trajectory inflections independently from where exactly the system is transiting (cf. Fig. 2). For lateral faces, trials approached the P1-template around [150, 350] ms; and the P400-template about [400, 600] ms post-stimulus onset. For the central faces, closest approach to ERP templates occurred, within the broad ranges between -150 and 150ms for the P1 template, and for the P400 template between 350 and 550ms (Fig. S4 B).

Secondly, latencies of ERP flybys tended to decrease with age, but not necessarily their variability (e.g. the jitter of flyby latencies to the P1 component even tended to increase with age, moderately but significantly, cf. Fig. 3B, S4 C-D and Table 1). Thirdly, the distance of flybys at the P1 component did not vary significantly with age, while there was a tendency for the distance at flybys to the P400 component to reduce (significantly for left and central but not for right faces, Fig. 3C, S4E-F and Tables 1 and 2). The variability of the flyby distances either remained unchanged, for the P1-template; or even grew with age, for the P400-template (Table 2). Fourthly, there were hemispheric asymmetries. Age effects in fly-by latency for left or centrally presented faces were not marked, but the same for the faces presented in the right hemifield were quite prominent (cf. Fig. S4 and Table 2). The effect of age on latencies for the right faces (processed by the left-hemisphere) shown in Fig. 3B was related to an initial delay in flyby latencies in the youngest infants. Thus, the "catch-up" relatively to the more mature right hemisphere during this period is congruent with several results showing a slower maturation of the left hemisphere compared to right (Chiron et al., 1997). Similar catch-up of the maturation of the left dorsal linguistic pathway relative to the right has also been described during the first semester post-term (Leroy et al., 2011).

We also verified that the trends found in Table 2 were not the artifactual manifestation of maturation in single-subject ERP templates, rather than maturation in variability. To check for this, we repeated flyby analyses using subject-specific ERP templates rather than grand-average templates (see *Methods* and Fig. S5A). As shown in Fig. S5B, all trends in Table 2 were reproduced even in this case, apart from the increase in latency jitter for the P1 component that was not anymore significant.

Altogether, these results, suggest that variability and loose relation to ERP templates may not be a "bug" of early infancy to correct for, but a feature preserved and evolving through development (see *Discussion*).

Between-trial variability quenching after stimulus presentation

Irrespective of their approach to the templates, trials can remain far or close to each other at any point. Hence, we investigated between-trial variability. Again, we found that trajectories remained highly dissimilar, as denoted by an average correlation distance of 0. 95 ± 0. 12 between the time-aligned trajectories of different trials. Although large in absolute terms, the between trials distance relatively reduced at specific peri-stimulus times. We observed a significant post-stimulus decrease in the between trial variability for all task-conditions and for both infants and adults (Blue plots in Fig. 4A-B, Fig. S6). For infants, between-trial variability significantly remained ~1-2. 5 standard deviations lower than the average baseline variability ~200-700ms post-stimulus (p = 0. 001 for left, right faces and p = 0. 003 for the central faces), while in adults, significant Variability Quenching (VQ) occurred ~150-500ms (p = 0. 005), similar to the duration previously reported for variability quenching in adults (Schurger et al., 2015).

Between-trial variability quenching is not automatically induced by ERP component flybys

The latency of the largest post-stimulus VQ (lowest variability) significantly differed across age-groups and task conditions. Strikingly, for lateralized faces, the latency of the significant VQ coincided with the latency of the closest P1-flyby in the youngest infants (First trimester: 5-12 week-old infants, N = 14) whereas in the older infants (Second Trimester: 16-24 weeks, N = 13), the moments of VQ co-occurred with

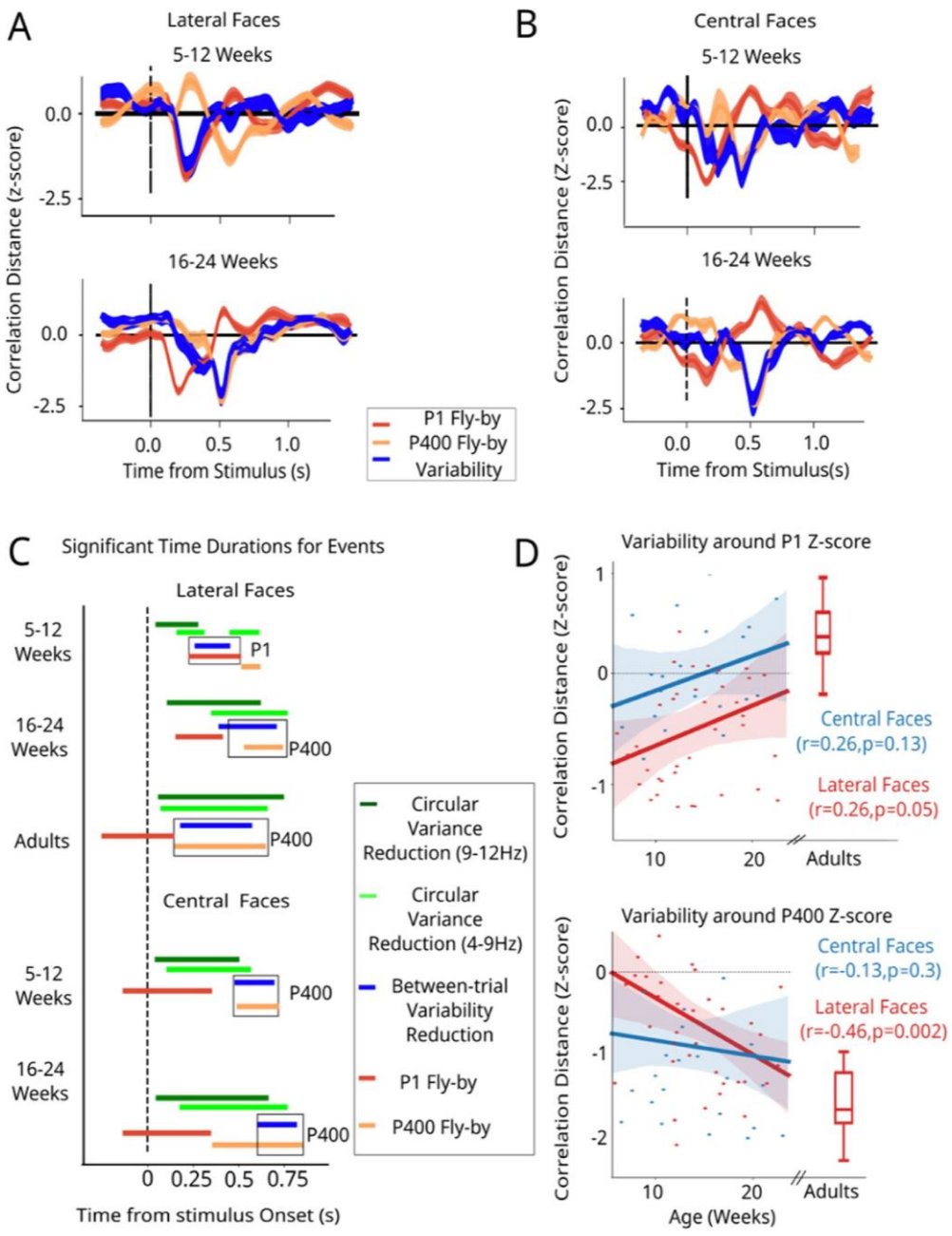

Fig. 4. Maturation of Between-trial variability and its relation to Flyby distances. A) Group average between-trial correlation distance (blue curves, Z-scored) for 5–12-week-old infants (top panel) and 16–24-week-old infants (bottom panel) plotted together with grand-average flyby distances (Z-scored) to P1 (red line) and P400 templates (orange line), for the lateral faces. Significant reduction in between-trial variability coincides with the closest-flyby to P1-template for 5-12wo infants (top panel), and with the P400-template for 16-24wo infants (bottom panel). **B)** For central faces, significant between-trial variability (blue line) reduction coincides with P400-flyby (orange line) for both groups. Shaded areas indicate standard error to the mean. **C**) Synoptic view, across conditions and age groups, of the time ranges when between-trial variability (blue), between-trial circular variance of phases of theta and alpha oscillations (light green and green respectively) and flyby distance (red /orange) are significantly reduced (Horizontal bars indicate timepoints of significant reductions from mean; $p<0.05$, corrected using cluster-based permutation t-test). Boxes highlight correspondence between clusters of between-trial variability and P1/P400 flyby distance reductions in different conditions. 16-24 wo infants qualitatively look like adults. 5-12 wo infants when presented with central faces also quench variability at P400 but at P1 for lateralized faces. In all conditions, Circular Variance (CV) reduction precedes variability quenching (VQ) events. **D)** Between-trial variability during P1-flyby positively correlated with age (top) while the same during P400-flyby negatively correlated with age for lateral but not central faces. (All r-values corrected for multiple comparison with one-tailed permutation test). Shaded area indicates 95 % confidence interval for regression estimates. Box-plots show between-trial variability distributions for adults.

the P400-flyby (Fig. 4A). In other words, in younger infants, the bundle of single trial trajectories remained on an average more compact when flying by the P1-template (significant VQ times: 204-352ms, window of closest P1-flyby: 175-400ms). By contrast, in older infants, trials remained the closest to each other when passing near the P400-template (significant VQ: 432 – 616ms, closest P400-flyby: 432-620ms).

Importantly, the absence of between-trial VQ did not imply absence of a flyby. Indeed, in first-trimester infants, trials still had a marked P400-flyby even when there was no between-trial VQ at the correspond- ing latency. Analogously, there was still a P1-flyby for second-trimester infants despite the lack of a P1 VQ. These effects were consistent for both left and right face presentation (Fig. S6A-B). Fig. S7A further confirmed that these effects were not methodological artifacts dependent on the choice of window-length for temporal smoothing, but was robust against such manipulation, i.e. same qualitative effects were present without any temporal smoothing and for a range of different sliding window widths.

Thus, flying by an ERP component appears to be a necessary but not a sufficient condition for between-trial VQ. In adults too, a single window of VQ coincided with the P400-flyby, like the second-trimester infants' pattern (Fig. 4C, Fig. S6 C-D). However, the VQ was much larger in adults than in infants, trials remaining significantly close to each other during the entire duration of the P400-flyby (significant VQ: 140 – 460ms, P400-Flyby: 120-528ms).

Between-trials variability quenching depends on both stimulus configuration and age

The temporal shift of the between-trial VQ, from P1 to P400 gives the first proof of a change in the ongoing dynamics occurring over the first semester of life. However, such a shift may also be due to the structural changes in the peripheral visual pathway and visual cortex V1 which are known to reach a milestone around 12 weeks post-term (Braddick and Atkinson, 2011; McCulloch et al., 1999; Adibpour et al., 2018). To in-

Table 3
Between-trial variability (z-scores) were compared for the three age-groups (5-12 wo, 16-24 wo and adults, group sizes as in Table 1) in their respective moments of P1 and P400 closest flybys using separate Kruskal-Wallis tests for different ERP templates (P1, P400) and for faces presented in the left and right hemi-field. The main effects are reported before post-hoc Mann-Whitney U-test for pair-wise comparisons. P-values are corrected for multiple comparisons using Bonferroni correction.

Age Difference in Between-trial Variability around Flybys (z-scores)		
	Left Faces	Right Faces
P1	H (2) = 11. 72, p = 0. 003	H (2) = 12. 95, p = 0. 001
	5-12 wo vs 16-24 wo: p = 0. 25n. s.	5-12 wo vs 16-24 wo: p = 0. 5 n. s.
	5-12 wo vs adults: p = 0. 003	5-12 wo vs adults: p = 0. 002
	16-24 wo vs adults: p = 0. 229 n. s.	16-24 wo vs adults: p = 0. 05
P400	H (2) = 16. 68, p = 0. 0002	H = 14. 10 (2), p = 0. 0009
	5-12wo vs 16-24 wo: p = 0. 001	5-12 wo vs 16-24 wo: p = 0. 08 n. s.
	5-12 wo vs adults: p = 0. 001	5-12 wo vs adults: p = 0. 002
	16-24 wo vs adults: p = 0. 8 n. s.	16-24 wo vs adults: p = 0. 1 n. s.

Table 4
Correlation trends with age of the strength of between-trial variability quenching, for right, left and centrally presented faces. The letter *r* denotes Pearson correlation and the letter □ Spearman rank-based correlation. Only significant correlations are indicated (i.e. 95% confidence interval not containing 0, for both types of correlations). None of the age-correlations of variability quenching strength for central faces significant (hence the missing table column).

Correlations between strength of between-trial variability quenching and age		
	Right faces	Left faces
P1	–	–
	–	–
P400	r = -0. 35, p = 0. 03, 95% c. i. [-0. 6, -0. 04]	r = -0. 43, p = 0. 003, 95% c. i. [-0. 65, -0. 13]
	□ = -0. 34, p = 0. 04, 95% c. i. [-0. 59, -0. 03]	□ = -0. 45, p = 0. 004, 95% c. i. [-0. 67, -0. 15]

vestigate the possible origin of such a shift, we repeated the same analysis in the subset of infants who were also presented with central faces (Fig. 4B). We found that the VQ at P1 but not P400-flyby significantly differed in the same infant for the two different face stimuli configurations (Wilcoxon signed rank z (21, 1) = 58, p = 0. 025 for P1, z (21, 1) = 123, p = 0. 92 for P400). This result remained unaffected when comparing central and lateral faces by equalizing the number of trials across conditions, confirming that the difference of variability quenching across conditions was not due to the difference in number of trials (Wilcoxon signed rank z (21, 1) = 46, p = 0. 007 for P1, z (21, 1) = 31, p = 0. 001 for P400). Interestingly, when presenting central face stimuli, the 5-12 weeks infants now showed a significant VQ at the P400-flybys, similarly to the response to lateral faces observed in 16-24 weeks infants. The absence of VQ at P400 for lateral faces in 5-12 weeks infants thus, does not reflect uniquely a poor maturation of connection pathways.

Fig. 4C summarizes the time-ranges of between-trials variability quenching and P1/P400-flybys across all experimental conditions and age groups ($p<0.05$, all analyses were corrected for multiple comparison and temporal independence using one-sided cluster-based permutation t-test). Age affected not only the latency but also the strength of VQ events, in similar directions for both stimulus configurations. Quenching strength decreased with age within the P1-range and increased within the P-400 range (Fig. 4D), with both these trends confirming the observed inter-group differences. Specifically, we found a linear increase of the strength of between-trials variability quenching with age at the P400-flyby latency for lateral faces, significant for left and right, but not central, faces (Fig. 4D, see Table 4 for Pearson and Spearman correlation values and confidence intervals). Table 3 and the box plots in Fig. 4D show that adult values further continue the trends observed in infancy.

Between-trials variability quenching is not equivalent to phase reset dynamics

EEG responses have oscillatory components, with a spectral resonance in the alpha band (9-12 Hz) which was relatively prominent peak in adult subjects, but way less marked in infants (Fig. S8A). To investigate the relation between VQ and reconfiguration of alpha oscillatory dynamics, we narrow-band filtered the EEG signals in two bands of interest corresponding to the adult "alpha" and "theta" (or "infant alpha") range (respectively, 9-12 Hz and 4-9 Hz) and extracted phase and amplitude of the oscillations through Hilbert transform (see Methods). Fig. S8 reports analyses about the standard "alpha" band and Fig. S9 about the lower frequency "theta" band. We first quantified the time-courses of trial-averaged power modulations (Fig. S8B, top and Fig. S9A) as well as the circular variance (CV) of phases across time-aligned trials (Fig. S8B, bottom and Fig. S9B). Average alpha power was not significantly modulated in the peri-stimulus duration in infants and was slightly but significantly reduced in adults (-12% below the baseline from [0, 656] ms, p = 0. 007, permutation cluster test).

The effect of stimulus presentation was slightly more pronounced on the oscillation phases. The measured CV across stimulus-aligned trials denoted a poor phase-alignment between-trials, with an average value of ~0. 80 (± 0. 06) in infants and ~0. 93 (± 0. 02) in adults, close to the unit value that would correspond to a complete asynchrony of phases across trials. Although face presentation did not fully reset ongoing oscillations, the CV significantly dropped in specific time-ranges following the stimulus, to values ~0. 4 S. D. below its mean for infants and ~1. 5S. D. below the mean for adults in both frequency bands (Fig. S8B, Fig. S9B).

Remarkably, CV drop and VQ had partially dissociated spatiotemporal dynamics in infants. In most infant subjects, drops of "alpha" phase CV tended to *precede* VQ (cf. peak with a negative latency in the cross-correlogram between the time-courses of VQ and "alpha" CV, Fig. S8D). Moreover, in infants, significant VQ episodes lasted longer (Fig. 4C, dark green lines) and affected a spatially more extended set of channels (see topographies in Fig. S8C, VQ at ~35% of channels vs CV drop at ~10% in infants). The CV drops, occurring in largely overlapping ranges for the two bands, were quantitatively larger for the "theta" range (to values ~0. 5-0. 7 S. D. below its mean for infants and ~2S. D. below its mean for adults) and more synchronized with VQ events (compare cross-correlation peaks in Fig. S9C vs Fig. S8D). However, in both cases, the timing relations were loose (peak cross-correlation at only ~0. 1).

These results collectively suggest the existence of a rich temporal structure in the dynamics of between-trials variability, qualitatively and quantitatively maturing over the first semester post-term birth. Furthermore, in the same infants, its temporal structure can be modulated depending on the task at hand. For infants, phase reset and VQ are intertwined but distinct events: substantial VQ can exist even in the absence of an increased phase alignment between trials as made clear by analyses of variability dynamics.

Absolute within-trial variability increases with age

Our third and last approach was the analysis of within-trial variability (the only one that, not requiring information from multiple trials at a time could inform us about features potentially relevant for actual neural computations, see *Discussion*). To track within-trial variability, we quantified the amount of variation in the topography of EEG activation from one time-point to the next. This corresponds to the distance traveled in the space of possible activity topographies over a unit time or, equivalently, to the *speed* of motion in this high-dimensional space (see Methods). With this approach, topographies of activation which are stable over time and fluctuate very little from one moment to the next will yield instantaneous within-trial variability close to zero. Conversely, abrupt changes of topographies occurring at specific instants – e.g. eventual switching between microstates (Michel & Koenig, 2018; cf.

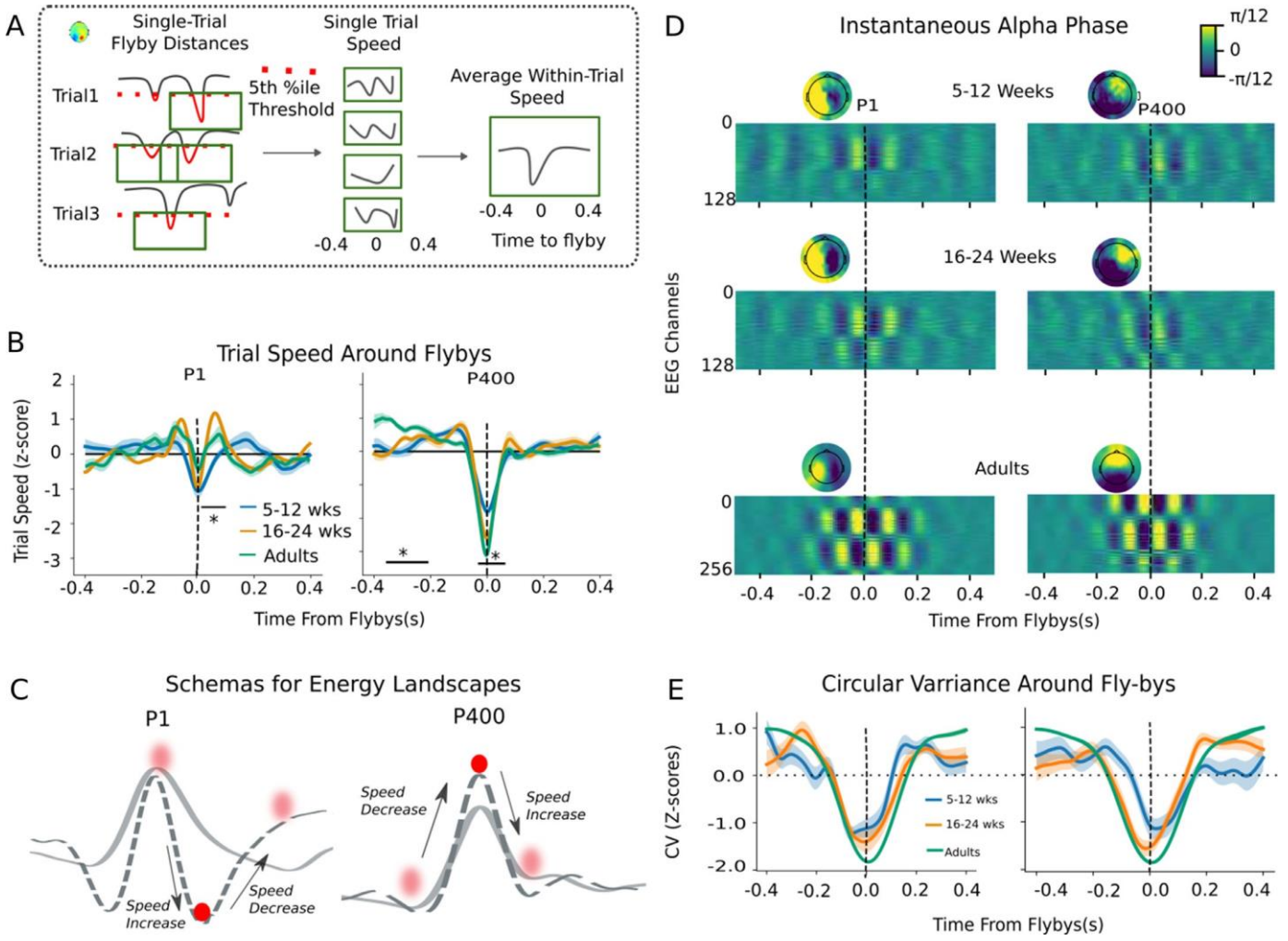

Fig. 5. Maturation of Within-trial Speed and its relation to alpha oscillations. A) Trial speed around P1 and P400 flyby events for each subject was extracted by considering within-trial speed (i.e. correlation distance between topographies from one time-point and next) in 800ms time-window around the closest 5 % flyby distances to the respective template. **B)** Group averaged trial speed profiles around P1 and P400 flybys for different age-groups. Significant speed difference existed between 5-12 weeks and 16-24 weeks old infants as indicated by black horizontal bars, cluster-based permutation t-test, $p<0.05$, permutation t-test without clustering for P400). **C)** Schematic energy landscapes that may underlie the speed profiles at P1 and P400 templates (solid line for 5-12 wo and dotted line for 16-24 wo infants respectively). The observed speed profiles could be interpreted as if motion along trajectories was driven by sampling of a structured potential energy landscape (like the rolling of a ball across hills and valleys on a surface). **D)** Group averaged flyby triggered instantaneous phase of alpha oscillations for each channel, separated by age-groups. Y-axis represents channels ordered according to their nomenclature. Topographies were derived by plotting instantaneous phase on the scalp surface at the first peak before the closest flyby for each age group. **E)** Circular Variance (CV) of alpha phases across closest flybys. As an effect of phase-reset preceding fly-by, CV dropped for all age groups in a range ~[-200, 200] ms surrounding the closest flyby. Shaded bars represent S. E. M. for each group.

Figs. 2C and S2) – would map to sudden increases of the instantaneous within-trial speed. Again, analogously to between-trial variability analyses, we related the changes of within-trial variability to the dynamics of "alpha" and "theta" band oscillations (Figs. 5 and S10).

We first measured average within-trial variability, irrespective of the time relative to stimulus presentation. We found that time-averaged absolute within-trial variability significantly increased with age for all task conditions (Fig. S10A (left panel) for lateral faces: r = 0. 38, p = 0. 01, 95% c. i. [0. 07, 0. 62]; (right panel) for central faces: r = 0. 56, p = 0. 009, 95% c. i. [0. 18, 0. 79]). Once again, this trend continued into adulthood, with a within-trial speed (or variability) significantly higher in adults compared to infants (box plot in Fig. S10A, H (2) = 24. 33, $p = 10^{-5}$, Kruskal-Wallis test). Thus, development boosted speed of exploration along neural trajectories.

We also noted, however, that within-trial speed was not homogeneous in time but had a heavy-tailed distribution of instantaneous values for both infants and adults (Fig. S10 B), with extreme values possibly reflecting long jumps due to microstate switching events. Given this heterogeneity of speed modulation in time, we then moved to study whether faster or slower speeds were systematically associated to specific neural configurations being visited, notably at ERP component flybys.

Speed profiles around ERP flybys are structured and modulated by age

To understand how within-trial speed is specifically modulated during the approach to known evoked ERP components, we first performed flyby-triggered averages of within trial speed of topography transitions from one moment to the next, by pulling together all individual events of closest flyby to ERP templates (possibly multiple events per trial) and averaging within-trial speed in an 800-ms window around these events (peri-flyby speed profiles, Fig. 5A, also see *Methods*). Fig. 5B shows average within-trial speed in the vicinity of respectively P1 and P400-flybys for lateral faces (Fig. S10C for central faces). In these profiles, peaks and troughs of within-trial speed are clearly visible, distributed symmetrically around the flyby time, and tend to get more prominent with age.

Table 5
Flyby triggered within-trial speed profile time-series (z-scores) across the three age-groups (5-12 wo, 16-24 wo infants and Adults, group sizes as in Table 1) were compared using cluster-based permutation F-tests separately for each ERP template and for each hemi-field to find the significant time clusters ($p<0.05$). During post-hoc analyses, average within-trial speed in these significant time-windows was compared using Kruskal-Wallis test. Pair-wise comparisons were tested using Mann-Whitney U-test. P-values are corrected for Bonferroni correction.

Age-differences in Within-Trial Variability Around Flybys		
	Left Faces	Right Faces
P1	S. C.: None	S. C.: [8 80] ms, H (2) = 6. 07, p = 0. 048 5-12 wo vs 16-24 wo: p = 0. 08 5-12 wo vs adults: p = 0. 17 16-24 wo vs adults: p = n. s.
P400	S. C.: [-384 -308] ms: H (2) = 14. 87, p = 0. 0006 5-12wo vs 16-24 wo: p = 0. 51n. s 5-12 wo vs adults: p = 0. 008 16-24 wo vs adults: p = 0. 0008	14. S. C. [-400 -268] ms, H (2) = 42, p = 0. 0007, = 0. 41 n. s 5-12wo vs 16-24 wo: p 5-12 wo vs adults: p = 0. 015 16-24 wo vs adults: p = 0. 0005 S. C. [-72 -12] ms, H (2) = 16. 266, p = 0. 0003 5-12wo vs 16-24 wo: p = n. s. 5-12 wo vs adults: p = 0. 0003 16-24 wo vs adults: p = 0. 03

S. C = Significant Clusters ($p<0.05$, cluster-based permutation tests)

Irrespective of their absolute within-trial speed, on an average, trials transiently slowed down around both P1 and P400-flybys, for all conditions and age-groups (always significantly, except for P1 flyby in adults, Table 5). These results remained qualitatively robust even when no temporal smoothing was applied to the single-trial topographic patterns as well as for range of different lengths of sliding window smoothing (Fig. S7B). Although the sliding window length determined the upward and downward slopes of within-trial speed curves at the time of flyby, significant age-difference existed in these curves for first and second trimester infants in all except for very large smoothing window (180ms, where the two curves were smudged). Slowing down was larger around P400-flyby than for P1 (condition-paired signed rank test: H (2) = 30, p = 0. 001, H (2) = 55, p = 10^{-5} and H (2) = 1. 0, p = 0. 0005 for infant central, lateral, and adult lateral faces respectively). As shown by Fig. S10D-F (left panels), speed of exploration nearby P1 flybys increased with age, significantly for lateral faces; but not for central faces (age correlation: r = 0. 47, p = 0. 001, 95% c. i. [0. 18, 0. 68] for left, r = 0. 35, p = 0. 02, 95% c. i. [0. 04, 0. 6] for right and r = 0. 1, p = 0. 7, 95% c. i. [-0. 34, 0. 5] for central faces). This increase was due to the emergence of more marked positive acceleration, preceding and following the time of closest flyby. On the contrary, speed of exploration decreased with age nearby P400 flybys, due to a progressively marked deceleration, for both lateral and central faces (respectively, Fig. S10D-E right panels, age correlation: r = -0. 45, p = 0. 001, 95% c. i. [-0. 67, -0. 16]for left, r = -0. 45, p = 0. 001, 95% c. i. [-0. 67, -0. 16] for right and r = -0. 33, p = 0. 07, 95% c. i. [-0. 66, 0. 11] for central faces, not significant, though, for this latter).

These characteristic speed profiles are reminiscent of the accelerations and decelerations that a physical ball would experience when rolling on a non-flat surface, accelerating while descending into a valley and decelerating while ascending out of the valley due to gravity (see illustration in Fig. 5C). It is thus tempting to interpret these speed profiles as if reflecting the sampling of a structured "energy landscape" (Ezaki et al., 2017; Gu et al., 2018). In this statistical physics-like view, neural trajectories would unroll under the influence of force fields generated by an effective potential, due to underlying but unspecified constraints in collective neural dynamics. These forces act as biases on the system's trajectory in the proximity of critical points associated to ERP components. Through development, this energy landscape gets progressively more sculpted, and the neural trajectories can be thought of as being more actively controlled (see *Discussion*).

ERP flybys are associated with transient phase reset but not amplitude modulation events

As in the case of between-trial variability, modulations of single-trial oscillatory dynamics may be an important contribution to the observed variations of the within-trial speed. We thus analyzed phase dynamics in the surrounding of fly-by events. In Fig. 5D we show for all channels flyby-triggered averages of the phase of "alpha" oscillations. In the surrounding of the closest flyby time, oscillatory patterns can be clearly distinguished, suggesting that flyby events tend to occur at similar instantaneous "alpha" phase. These analyses thus provide evidence for phase reset in the surrounding of the flybys: (i) for all age groups; and, (ii) with a distinct global topography for each ERP component. This phase alignment between the oscillations at different ERP flybys begins ~200ms before the flyby event and ends around the same time after the flyby. This indicates that fly-by events are not the cause of reset (otherwise, oscillatory patterns would be visible in the average phase time-series only *after* the fly-by). On the contrary, fly-by arise dominantly at a specific phase during a *pre-existing* oscillatory event, and the number of cycles visible in the fly-by triggered averages of Fig. 5D before and after the fly-by are just indicative of the average duration of regular oscillatory episodes (i.e. intrinsic decorrelation time of ongoing oscillations). In line with this phase alignment of alpha oscillations to ERP component flybys, the flyby-triggered Circular Variance (CV) of "alpha" phase across single-flyby events also dropped significantly (Fig. 5E). A qualitatively similar dynamics occurred for "theta" oscillations, with an even larger CV drop (Fig. S9D).

Importantly, within-trial speed modulations were paralleled by phase modulations but not as clearly by amplitude modulations. Considering the amplitude of the signal "alpha" component, alpha power surrounding ERP flybys did not significantly deviate from baseline values for any of the groups (Fig. S11A). These results hold also for the "theta" band. Indeed, more in general, beyond band-restricted oscillatory dynamics, it is broadband power which appears poorly modulated by stimulus and flybys. We considered more general modulations of signal-to-noise ratio, by quantifying the L2-norm of the topography of activation to track average activity levels at all channels. Averages of L2-norm of activation over stimulus-aligned trials did not show any significant upward or downward modulation in any time range following the stimulus (Fig. S11B, neither for lateral faces (top panel), nor for central faces (bottom panel)). This corresponds to the fact that strong voltage activity can be found at any time within individual trials, due to ongoing fluctuations (cf. Fig. 2A-C) and are not restricted to the classic ERP time-ranges. As shown by Fig. S11C, we again found flat profiles of L2-norm change around flyby events for most combinations of age and stimulus type (the only exception being a significant increase at P400-flyby, limited to the adult group).

Discussion

In this study, we demonstrate the existence of a rich temporal organization of the neural responses to stimulus in adults and infants that goes beyond the mean response captured by ERPs. We propose the concept of Event-Related Variability (ERV) to refer to the temporally structured dynamics of the response fluctuations. To characterize ERV, we focused on the complementary aspects of: single-trial (dis)-similarity to known ERP components (ERP flyby analyses, Fig. 3); reproducibility of response trajectories across different trials (between-trials variability analyses, Fig. 4); and speed of reconfiguration of the induced activity topographies along individual trials (within-trial speed analyses, Fig. 5). We furthermore put these three aspects in relation with the dynamics of

ongoing oscillations to study the contribution of phase reset to ERP flybys and variability quenching. Our results confirm that, for both infants and adults, the trial variability remains very large and that stimulus presentation does not suppress ongoing fluctuations. Yet this variability is significantly modulated by face presentation in a non-trivial way, as exposed by the ERP flybys and variability quenching.

In all conditions, a period of decreased variability across trial trajectories (variability quenching) is detected after stimulus presentation, confirming many previous reports in adults (Ito et al., 2020; Arazi et al., 2017; Schurger et al., 2015; Schurger et al., 2010). Beyond these previous studies, we observe that the time-range of between-trial variability quenching evolves through age and that, at a given age, is strongly and qualitatively modified by the task at hand. Furthermore, we observe that variability quenching always occurs in time ranges in which trials approach ERP landmark topographies (ERPs flybys). The converse however is not true (cf. Fig. 4). This establishes ERP flybys and between-trial variability quenching as partly independent phenomena. Variability quenching (VQ) is also partially independent of the phase reset of ongoing oscillations. Thus, reset of oscillatory dynamics may be only one facet of the complex variability modulations that system's response trajectories experience in response to a stimulus.

Might Variability Quenching denote Top-down Processes?

Various elements suggest that quenching events are not a mere automatic consequence of stimulus presentation, but might signal a more controlled system's trajectory, possibly implementing a form of top-down regulation: First, quenching could occur late after the stimulus onset, for example ~400-600ms, i.e. in P400 time-window in older infants. Second, age did not simply extend the time-window of quenching but shifted its target, from P1 to P400, and third, even at a given age, the quenching dynamics was qualitatively modified by changes in the stimulus configuration. First-trimester infants showed P1-component flybys for both central and lateral faces, but variability quenching at P1 flyby occurred only for lateralized faces, i.e. for the most challenging task. Indeed, lateralized faces were much more difficult to perceive because they were presented briefly at a random interval and in a competition with the central attractor that helped avoid infants' saccades. Moreover, the slow maturation of parafovea compared to fovea (Allen et al., 1996) made this brief lateral stimulus even less discernible for the younger infants. We hypothesize that variability quenching events through top-down control processes helped the infants' guide their attention in the absence of a strong bottom-up signal. For e.g. younger infants might try to shift their attention towards the lateralized stimuli in order to "detect" it, without recognizing a specific face, or even extracting facial features, while the older infants and adults might focus their attention on guessing/recognizing the face, thus quenching variability at a later stage of processing. This could explain the shift of variability quenching from the P1 component (related merely to the detection of the visual input) to the P400 ERP component that is related to the face processing. Similarly, when the face was centrally presented, younger infants could also focus on the face identity, the detection part being plainly evident. From this interpretation, a quenching event (that indicates a transient constraining of the system's dynamics to a specific trajectory) might reflect *more intensive information processing* than the "hit and run" visit to the P1-component observed in older participants and in the case of an easily perceived visual event (central faces) for younger participants. The existence of top-down regulatory mechanisms in infants has been confirmed experimentally (Emberson et al., 2015; Kabdebon and Dehaene-Lambertz, 2019; Kouider et al., 2015). Notably, the shift of focus for variability quenching, from P1 to P400 after 12 weeks for lateral faces corresponds to the first milestone in visual development when several peripheral structures reach maturity (e.g. lens, fovea) and myelination of the optical fibers and maturation of V1 reach a plateau after a period of rapid change. These changes translate in the convergence to adult values of the P1 latency for centrally presented stimuli around 12 weeks (Dubois et al., 2008), while peripheral vision matures more slowly (Allen et al., 1996). Feed-back connectivity is also progressively restructured after term-birth (Kennedy et al., 2007), passing from disperse growth to selective pruning which may allow for more effective and selective attention control or predictive influences resulting into variability quenching at later stages for older infants. In future, task difficulty and information processing load should be parametrically adjusted to investigate their respective influence on ERV dynamics, from early infancy to adulthood.

Within-Trial Variability Modulation

Beyond the common focus on modulations of variability between trials, we emphasized variability modulation events taking place within individual trials. We confirmed previous results obtained for adults (Schurger et al., 2015) and extended them to infants. If a between-trial variability quenching event denotes that the flow of system's trajectories is restrained to a specific manifold when reaching and leaving an ERP component, the phenomenon of within-trial slowing-down suggests that the flow of *each of the individual trajectories* on this manifold characteristically decelerates when the system approaches certain landmarks (ERP component flyby). This is important, because perception and cognition happen in real time (without waiting for multiple stimulus presentations before perceiving a face). Therefore, instantaneous modulations of response variability can be instrumental only if they occur within individual trials. The slight slowing-down of individual trials near P1and, in a particularly marked way, P400-flybys, correspond to the system trajectories lingering in an orbit around the corresponding ERP template for a short time. Such transient slowing down (or speeding up when entering or leaving the orbit, as for P1 flybys) might be detected, by an integrator neuron –serving as a tempotron readout (Gütig & Sompolinsky, 2006) – to signal that a given stage in cognitive processing has been reached and thus initiate the next processing step in a sequence. These speed modulation profiles can remain well identifiable by the system, despite the large variability of spatial topographies at ERP flybys.

Together, our results suggest that more than the current position of the system in its configuration space, ERPs are marked by "how" the system is flowing through and away from its current position. The evolution of the system seems far from being at a stable attractor. The fact that dynamics is dominated by structured fluctuations make such a system compliant with reservoir computing systems, in which intrinsic chaotic fluctuations are only transiently reduced by the applied inputs and are needed to boost learning capabilities.

Mechanisms underlying Variability Modulations and their Possible Functional Relevance

The question remains as to what mechanisms could be responsible for the emergence of such a structured ERV components. This question has been explored in some depth for the quenching of firing rate variability in neuronal population responses to a stimulus where mechanisms such as attractor stabilization (Litwin-Kumar and Doiron, 2012), chaos suppression (Rajan et al., 2010) or "supra-linear stabilization" (Hennequin et al., 2018) have been proposed. Large-scale computational efforts (Ponce-Alvarez et al., 2015) have demonstrated that such microscopic properties could indeed be an ingredient for the macroscopic variability quenching, which are sampling a more global activity than the neural firing recordings reviewed by (Churchland et al., 2010). Contrarily, some studies have suggested that macroscopic quenching could be due to the variations in the baseline power and/or the phase of ongoing alpha oscillations(Jensen et al., 2012; Daniel et al., 2019; Wainio-ThebergeS and Northoff, 2021). These views are akin in spirit to earlier and more recent proposals that oscillatory phase and amplitude modulations are responsible for the generation of ERP components and their trial-to-trial fluctuations (Hanslmayr et al., 2007). Here we have found

however that variability quenching can persist longer even after the return to baseline levels of circular variance, especially in the younger infants. This means that neural response trajectories keep being restrained to a common manifold even when ongoing oscillations have decorrelated and are not anymore aligned in phase. More general forms of trajectory control may thus be acting, and oscillatory phase reset could be just an early component of them (causal trigger), or, alternatively, just their epiphenomenal manifestation.

Moreover, the characteristic kinematics of system's evolution was observed here as neural trajectories approach ERP components. Such type of kinematics and effective landscapes may naturally emerge because of the non-linear dynamics of multi-scale neural circuits, self-organizing into structured flows on low-dimensional manifolds (Pillai and Jirsa, 2017). Trajectory deflections at ERP component flybys (including phase reset for oscillatory trajectories, but not exclusively) could be conceptualized as driven by the sampling of a landscape of effective free energy. If the observed speed profiles had to be explained as due to motion in a force field associated to this landscape, then, the free energy minima (the troughs of the landscape valleys) would be located at the first maximum of speed, which precedes the time of closest passage near ERP templates by~50-100ms. Thus, ERP-like configurations, associated to the lowest speed, would not be the "attractors" but rather signal the moment of crossing from one critical point to the next.

In this framework, changes of ERV dynamics through development and learning would be accounted for by the growth of more marked barriers and sinks in the effective energy landscape or, equivalently, bifurcations causing the birth, fusion or death of different attractors or saddle points in the system's high dimensional phase space. Such conjectures may be potentially validated by estimating the morphology of an effective energy landscape surrounding the ERP templates (Ezaki et al., 2017). Like previous studies, we find here also the increase of overall within-trial variability along early development (Fig. S10A-B) (Garrett et al., 2011; McIntosh et al., 2010). This increased structur- ing of the landscapes that shaped the brain activity may mediate the capability to learn internal statistical models of environment, for bet- ter inferences in perception (Berkes et al., 2011). Additional theoretical and computational investigation will be needed to disambiguate which of the possible scenarios is leading to the observed quenching, possi- bly also linking them to maturation of the underlying excitatory and inhibitory local circuits.

To probe the functional relevance of ERV, a focus on an early developmental period (and, particularly, as early as the first trimester post-term birth), may be once again crucial. Indeed, learning in early infancy is exceptionally fast (Dehaene-Lambertz and Spelke, 2015). At the same time, ERV dynamics is already rich and still evolving yet separable from phenomena such as alpha modulations that are dominated in adults and may conceal subtler functional aspects of response variability.

Methodological Considerations

Our approach has methodological limitations that could be overcome by future developments. For instance, the extraction of ERP templates in our case depended on a manual inspection based on the developmental literature, but more sophisticated algorithms for the temporal clustering of single-trial ERP topographies could be used and combined with our variability analyses schemes (Vahid et al., 2020). The occurrence of large within-trial variations and particularly of extreme within-trial speed values at certain times (Fig. S10B) – also need to be put in correspondence with the scale-free dynamics of microstate transitions, neuronal avalanching (O'Byrne and Jerbi, 2022) or other approaches to describe spontaneous dynamics as random walks in high-dimensional state spaces (Hansen et al., 2015; Naik et al., 2017), which also correlate speed variations with development and cognitive performance (Battaglia et al., 2020; Lombardo et al., 2020) and are shaped by intrinsic dynamical landscapes. Finally, linking activity to network state dynamics –what is the functional connectivity triggered by an ERP flyby?– may allow assessing whether exchange of information is dominated by bottom-up or top-down flows at different ages or ERP stages. Note that our measures were very sensitive to age, allowing capturing even subtle differences between the left and right hemisphere maturational calendar. The ERV approach might thus be a more sensitive tool than classical ERPs to capture differences between experimental conditions in infant cognitive studies, but above all to explore neurodevelopmental disorders.

Conclusion

ERPs have been an attractive description of the post-stimulus brain activity, described as successive steps defined by their reproducible latency and brain sources, allowing obtaining neural algorithms underlying cognition. However, this description was somewhat misleading, ignoring the ongoing activity. The framework proposed here encompasses both aspects. We recovered that ERP components serve as a "compass" to identify special dynamical points for the on-going activity sampling erratically vast volumes of the neural configurations space, confirming that ERPs are indeed capturing neural consequences of a stimulus presentation. At the same time, we also showed that they are far from capturing the entire activity patterns following a stimulus. We proposed the term ERV, as a better concept to describe the neural consequences of a stimulus. This proposal is not purely semantic since it allows describing the ERP maturation in integrated manner on one hand and emphasizes the structured variability of the background EEG on the other. It allows thus speculating that the gradual change of ongoing activity might reflect the increasing knowledge of the environment throughout development of a structured internal landscape biasing neural trajectories (that, on their turn, through their volatility, can efficiently sample this landscape). This approach might be particularly fruitful to investigate neurodevelopmental disorders and their cognitive consequences.

Data and Code Availability Statement

All processed data will be available upon request to the authors at the corresponding author email address, together with python scripts for ERV analyses.

Declaration of Competing Interest

None.

Credit authorship contribution statement

Shruti Naik: Conceptualization, Formal analysis, Investigation, Validation, Visualization, Writing – original draft, Writing – review & editing. **Parvaneh Adibpour:** Data curation, Resources, Writing – review & editing. **Jessica Dubois:** Data curation, Resources, Writing – review & editing. **Ghislaine Dehaene-Lambertz:** Conceptualization, Funding acquisition, Project administration, Supervision, Validation, Visualization, Writing – original draft, Writing – review & editing. **Demian Battaglia:** Conceptualization, Funding acquisition, Project administration, Supervision, Validation, Visualization, Writing – original draft, Writing – review & editing.

Data availability

Data will be made available on request.

Acknowledgements

This research was supported by grants from the Fondation NrJ, from the European Research Council (ERC) under the European Union's Horizon 2020 research and innovation program (grant agreement No. 695710), and from the Fondation de France (call Neurodevelopment and

Autism 2012). This work, carried out in part within the Institut de Convergence ILCB (ANR-16-CONV-0002), has benefited from support from the French government, managed by the French National Agency for Research (ANR) and the Excellence Initiative of Aix-Marseille University (A* MIDEX). DB has been supported by the University of Strasbourg Institute for Advanced Studies (USIAS-2020-044) where part of this research has been conducted.

Supplementary materials

Supplementary material associated with this article can be found, in the online version, at doi:10.1016/j.neuroimage.2023.120208.

References

Adibpour, P, Dubois, J, Dehaene-Lambertz, G., 2018. Right but not left hemispheric discrimination of faces in infancy. Nat. Hum. Behav. 2 (1), 67–79.
Adrian, ED, Matthews, BHC., 1934. The interpretation of potential waves in the cortex. J. Physiol. 81 (4), 440–471.
Allen, D, Tyler, CW, Norcia, AM, 1996. Development of grating acuity and contrast sensitivity in the central and peripheral visual field of the human infant. Vision Res. 36 (13), 1945–1953.
Arazi, A, Censor, N, Dinstein, I., 2017. Neural variability quenching predicts individual perceptual abilities. J. Neurosci. 37 (1), 97–109.
Arazi, A, Yeshurun, Y, Dinstein, I., 2019. Neural Variability is Quenched by Attention. J. Neurosci. 39 (30), 5975–5985.
Baria, AT, Maniscalco, B, He, BJ., 2017. Initial-state-dependent, robust, transient neural dynamics encode conscious visual perception. PLoS Comput. Biol. 13 (11), e1005806.
Battaglia, D, Boudou, T, Hansen, ECA, Lombardo, D, Chettouf, S, Daffertshofer, A, et al., 2020. Dynamic functional connectivity between order and randomness and its evolution across the human adult lifespan. Neuroimage 222, 117156.
Berkes, P, Orbán, G, Lengyel, M, Fiser, J., 2011. Spontaneous cortical activity reveals hallmarks of an optimal internal model of the environment. Science (80-) 331 (6013), 83–87.
Braddick, O, Atkinson, J., 2011. Development of human visual function. Vision Res. 51 (13), 1588–1609.
Broday-Dvir, R, Grossman, S, Furman-Haran, E, Malach, R., 2018. Quenching of spontaneous fluctuations by attention in human visual cortex. Neuroimage 171, 84–98.
Chaudhuri, R, Gerçek, B, Pandey, B, Peyrache, A, Fiete, I., 2019. The intrinsic attractor manifold and population dynamics of a canonical cognitive circuit across waking and sleep. Nat. Neurosci. 22 (9), 1512–1520.
Chiang, AKI, Rennie, CJ, Robinson, PA, Van Albada, SJ, Kerr, CC., 2011. Age trends and sex differences of alpha rhythms including split alpha peaks. Clin. Neurophysiol. 122 (8), 1505–1517.
Chiron, C, Jambaque, I, Nabbout, R, Lounes, R, Syrota, A, Dulac, O., 1997. The right brain hemisphere is dominant in human infants. Brain 120 (6), 1057–1065.
Churchland, MM, Yu, BM, Cunningham, JP, Sugrue, LP, Cohen, MR, Corrado, GS, et al., 2010. Stimulus onset quenches neural variability: a widespread cortical phenomenon. Nat. Neurosci. 13 (3), 369–378.
Daniel, E, Meindertsma, T, Arazi, A, Donner, TH, 2019. Dinstein I. The relationship between trial-by-trial variability and oscillations of cortical population activity. Sci. Rep. 9 (1), 1–11.
De Haan, M, Johnson, MH, Halit, H., 2003. Development of face-sensitive event-related potentials during infancy: a review. Int. J. Psychophysiol. 51 (1), 45–58.
Dehaene, S, Posner, MI, Tucker, DM., 1994. Localization of a neural system for error detection and compensation. Psychol. Sci. 5 (5), 303–305.
Dehaene-Lambertz, G, Spelke, ES., 2015. The infancy of the human brain. Neuron 88 (1), 93–109.
Dubois, J, Dehaene-Lambertz, G, Soares, C, Cointepas, Y, Le Bihan, D, Hertz-Pannier, L, 2008. Microstructural correlates of infant functional development: example of the visual pathways. J. Neurosci. 28 (8), 1943–1948.
Emberson, LL, Richards, JE, Aslin, RN., 2015. Top-down modulation in the infant brain: Learning-induced expectations rapidly affect the sensory cortex at 6 months. Proc. Natl Acad. Sci. 112 (31), 9585–9590.
Ezaki, T, Watanabe, T, Ohzeki, M, Masuda, N., 2017. Energy landscape analysis of neuroimaging data. Philos. Trans. R Soc. A Math. Phys. Eng. Sci. 375 (2096), 20160287.
Freschl, J, Al Azizi, L, Balboa, L, Kaldy, Z, Blaser, E, 2022. The development of peak alpha frequency from infancy to adolescence and its role in visual temporal processing: a meta-analysis. Developmental Cognitive Neurosci. 57, 101146.
Foxe, JJ, Snyder, AC., 2011. The role of alpha-band brain oscillations as a sensory suppression mechanism during selective attention. Front. Psychol. 2, 154.
Garrett, DD, Kovacevic, N, McIntosh, AR, Grady, CL., 2011. The importance of being variable. J. Neurosci. 31 (12), 4496–4503.
Ghuman, AS, Brunet, NM, Li, Y, Konecky, RO, Pyles, JA, Walls, SA, et al., 2014. Dynamic encoding of face information in the human fusiform gyrus. Nat. Commun. 5 (1), 1–10.
Gramfort, A, Luessi, M, Larson, E, Engemann, DA, Strohmeier, D, Brodbeck, C, et al., 2013. MEG and EEG data analysis with MNE-Python. Front. Neurosci. 7, 267.
Gu, S, Cieslak, M, Baird, B, Muldoon, SF, Grafton, ST, Pasqualetti, F, et al., 2018. The energy landscape of neurophysiological activity implicit in brain network structure. Sci. Rep. 8 (1), 1–15.
Gütig, R, Sompolinsky, H., 2006. The tempotron: a neuron that learns spike timing–based decisions. Nat. Neurosci. 9 (3), 420–428.
Hansen, ECA, Battaglia, D, Spiegler, A, Deco, G, Jirsa, VK., 2015. Functional connectivity dynamics: modeling the switching behavior of the resting state. Neuroimage 105, 525–535.
Hanslmayr, S, Klimesch, W, Sauseng, P, Gruber, W, Doppelmayr, M, Freunberger, R, et al., 2007. Alpha phase reset contributes to the generation of ERPs. Cereb. Cortex 17 (1), 1–8.
He, BJ., 2013. Spontaneous and task-evoked brain activity negatively interact. J. Neurosci. 33 (11), 4672–4682.
Hennequin, G, Ahmadian, Y, Rubin, DB, Lengyel, M, Miller, KD., 2018. The dynamical regime of sensory cortex: stable dynamics around a single stimulus-tuned attractor account for patterns of noise variability. Neuron 98 (4), 846–860 e5.
Hensch, TK, Fagiolini, M., 2005. Excitatory–inhibitory balance and critical period plasticity in developing visual cortex. Prog. Brain Res. 147, 115–124.
Hesselmann, G, Kell, CA, Eger, E, Kleinschmidt, A., 2008. Spontaneous local variations in ongoing neural activity bias perceptual decisions. Proc. Natl Acad. Sci. 105 (31), 10984–10989.
Hill, AT, Clark, GM, Bigelow, FJ, Lum, JAG, Enticott, PG., 2022. Periodic and aperiodic neural activity displays age-dependent changes across early-to-middle childhood. Dev Cogn Neurosci 54, 101076.
Huk, A, Bonnen, K, He, BJ., 2018. Beyond trial-based paradigms: Continuous behavior, ongoing neural activity, and natural stimuli. J. Neurosci. 38 (35), 7551–7558.
Iemi, L, Busch, NA, Laudini, A, Haegens, S, Samaha, J, Villringer, A, et al., 2019. Multiple mechanisms link prestimulus neural oscillations to sensory responses. Elife 8, e43620.
Ito, T, Brincat, SL, Siegel, M, Mill, RD, He, BJ, Miller, EK, et al., 2020. Task-evoked activity quenches neural correlations and variability across cortical areas. PLoS Comput. Biol. 16 (8), 560730.
Jasper, HH., 1937. Electrical signs of cortical activity. Psychol. Bull. 34 (7), 411.
Jensen, O, Bonnefond, M, VanRullen, R., 2012. An oscillatory mechanism for prioritizing salient unattended stimuli. Trends Cogn. Sci. 16 (4), 200–206.
Jung, T, Makeig, S, Westerfield, M, Townsend, J, Courchesne, E, Sejnowski, TJ, 2001. Analysis and visualization of single-trial event-related potentials. Hum. Brain Mapp. 14 (3), 166–185.
Kabdebon, C, Dehaene-Lambertz, G., 2019. Symbolic labeling in 5-month-old human infants. Proc. Natl Acad. Sci. 116 (12), 5805–5810.
Kenet, T, Bibitchkov, D, Tsodyks, M, Grinvald, A, Arieli, A., 2003. Spontaneously emerging cortical representations of visual attributes. Nature 425 (6961), 954–956.
Kennedy, H, Douglas, R, Knoblauch, K, Dehay, C., 2007. Self-organization and pattern formation in primate cortical networks. Novartis Foundation Symposium. Wiley Online Library; 178.
Klimesch, W., 2012. Alpha-band oscillations, attention, and controlled access to stored information. Trends Cogn. Sci. 16 (12), 606–617.
Kouider, S, Long, B, Le Stanc, L, Charron, S, Fievet, AC, Barbosa, LS, et al., 2015. Neural dynamics of prediction and surprise in infants. Nat. Commun. 6, 1–8.
Kutas, M, Federmeier, KD., 2000. Electrophysiology reveals semantic memory use in language comprehension. Trends Cogn. Sci. 4 (12), 463–470.
Leroy, F, Glasel, H, Dubois, J, Hertz-Pannier, L, Thirion, B, Mangin, JF, 2011. De- haene-Lambertz G. Early maturation of the linguistic dorsal pathway in human in- fants. J. Neurosci. 26 (4), 1500–1506 31.
Litwin-Kumar, A, Doiron, B., 2012. Slow dynamics and high variability in balanced cortical networks with clustered connections. Nat. Neurosci. 15 (11), 1498–1505.
Lombardo, D, Casse-Perrot, C, Ranjeva, J-P, Le, Troter A, Guye, M, Wirsich, J, et al., 2020. Modular slowing of resting-state dynamic Functional Connectivity as a marker of cognitive dysfunction induced by sleep deprivation. Biorxiv 2020 01. 17. 910810.
Marshall, PJ, Bar-Haim, Y, Fox, NA., 2002. Development of the EEG from 5 months to 4 years of age. Clin. Neurophysiol. 113 (8), 1199–1208.
Mazor, O, Laurent, G., 2005. Transient dynamics versus fixed points in odor representations by locust antennal lobe projection neurons. Neuron 48 (4), 661–673.
McCulloch, DL, Orbach, H, Skarf, B., 1999. Maturation of the pattern-reversal VEP in human infants: a theoretical framework. Vision Res. 39 (22), 3673–3680.
McIntosh, AR, Kovacevic, N, Lippe, S, Garrett, D, Grady, C, Jirsa, V, 2010. The development of a noisy brain. Arch. Ital. Biol. 148 (3), 323–337.
Michalareas, G., Vezoli, J., Pelt, S.van, Schoffelen, J.-M., Kennedy, H., Fries, P, 2016. Alpha-beta and gamma rhythms subserve feedback and feedforward influences among human visual cortical areas. Neuron 89, 384 397.
Michel, CM, Koenig, T., 2018. EEG microstates as a tool for studying the temporal dynamics of whole-brain neuronal networks: a review. Neuroimage 180, 577–593.
Naik, S., Subbareddy, O., Banerjee, A., Roy, D., Bapi, R. S., 2017. May). Metastability of cortical BOLD signals in maturation and senescence. In: *2017 International Joint Conference on Neural Networks (IJCNN)*. IEEE.Chicago, pp. 4564–4570.
O'Byrne, J, Jerbi, K., 2022. How critical is brain criticality? Trends Neurosci. 45 (11), 820–837.
Palva, S, Palva, JM., 2007. New vistas for □-frequency band oscillations. Trends Neurosci. 30 (4), 150–158.
Pezzulo, G., Zorzi, M., Corbetta, M., 2021. The secret life of predictive brains: what's spontaneous activity for? Trends Cogn. Sci. 25, 730–743.
Pillai, AS, Jirsa, VK., 2017. Symmetry breaking in space-time hierarchies shapes brain dynamics and behavior. Neuron 94 (5), 1010–1026.
Ponce-Alvarez, A, He, BJ, Hagmann, P, Deco, G., 2015. Task-driven activity reduces the cortical activity space of the brain: experiment and whole-brain modeling. PLoS Comput. Biol. 11 (8), e1004445.
Posner, MI, DiGirolamo, GJ., 2000. Cognitive neuroscience: Origins and promise. Psychol. Bull. 126 (6), 873.
Rajan, K, Abbott, LF, Sompolinsky, H., 2010. Stimulus-dependent suppression of chaos in recurrent neural networks. Phys. Rev. E 82 (1), 11903.
Sadaghiani, S, Hesselmann, G, Kleinschmidt, A., 2009. Distributed and antagonistic contributions of ongoing activity fluctuations to auditory stimulus detection. J. Neurosci. 29 (42), 13410–13417.

Schurger, A, Pereira, F, Treisman, A, Cohen, JD., 2010. Reproducibility distinguishes conscious from nonconscious neural representations. Science (80-) 327 (5961), 97–99.
Schurger, A, Sarigiannidis, I, Naccache, L, Sitt, JD, 2015. Dehaene S. Cortical activity is more stable when sensory stimuli are consciously perceived. Proc. Natl Acad. Sci. 112 (16), E2083–E2092.
Skrandies, W., 1990. Global field power and topographic similarity. Brain Topogr. 3 (1), 137–141.
Stroganova, TA, Orekhova, EV, Posikera, IN., 1999. EEG Alpha Rhythm in Infants. Clin. Neurophysiol. 110 (6), 997–1012.
Vahid, A, Mückschel, M, Stober, S, Stock, A-K, Beste, C., 2020. Applying deep learning to single-trial EEG data provides evidence for complementary theories on action control. Commun. Biol. 3 (1), 1–11.
Van de Ville, D, Britz, J, Michel, CM., 2010. EEG microstate sequences in healthy humans at rest reveal scale-free dynamics. Proc. Natl Acad. Sci. 107 (42), 18179–18184.
Van Diepen, RM, Cohen, MX, Denys, D, Mazaheri, A., 2015. Attention and temporal expectations modulate power, not phase, of ongoing alpha oscillations. J. Cogn. Neurosci. 27 (8), 1573–1586.
Van Dijk, H, Schoffelen, J-M, Oostenveld, R, Jensen, O., 2008. Prestimulus oscillatory activity in the alpha band predicts visual discrimination ability. J. Neurosci. 28 (8), 1816–1823.
VanRullen, R, Busch, N, Drewes, J, Dubois, J., 2011. Ongoing EEG phase as a trial-by-trial predictor of perceptual and attentional variability. Front. Psychol. 2, 60.
Wainio-ThebergeS, Wolff A, Northoff, G, 2021. Dynamic relationships between spontaneous and evoked electrophysiological activity. Commun. Biol.. 2021 (4), 1 1-17.
Zylberberg, A, Dehaene, S, Roelfsema, PR, Sigman, M., 2011. The human Turing machine: A neural framework for mental programs. Trends Cogn. Sci. 15 (7), 293–300.

Further readings

Dinstein, I, Heeger, DJ, Behrmann, M., 2015. Neural variability: friend or foe? Trends Cogn. Sci. 19 (6), 322–328.
Kirst, C, Timme, M, Battaglia, D., 2016. Dynamic information routing in complex networks. Nat. Commun. 7 (1), 1–9.